JGR Atmospheres

RESEARCH ARTICLE
10.1029/2022JD037434

The Wet Bias of RegCM4 Over Tibet Plateau in Summer Reduced by Adopting the 3D Sub-Grid Terrain Solar Radiative Effect Parameterization Scheme

Chunlei Gu[1], Anning Huang[1], Yaocun Zhang[1], Ben Yang[1], Shuxin Cai[1], Xiaoke Xu[1], Jiangxin Luo[1], and Yang Wu[1]

[1]School of Atmospheric Sciences, Nanjing University, Nanjing, China

Key Points:

- A 3-dimensional sub-grid terrain solar radiative effect (3DSTSRE) scheme has been successfully implemented into the RegCM4 model
- The surface solar radiation flux and heat balance over the Tibetan Plateau in summer can be clearly improved by RegCM4 with the 3DSTSRE
- The wet biases of RegCM4 over the regions with complex terrain in Tibetan Plateau can be largely reduced by adopting the 3DSTSRE scheme

Correspondence to:
A. Huang,
anhuang@nju.edu.cn

Citation:
Gu, C., Huang, A., Zhang, Y., Yang, B., Cai, S., Xu, X., et al. (2022). The wet bias of RegCM4 over Tibet Plateau in summer reduced by adopting the 3D sub-grid terrain solar radiative effect parameterization scheme. *Journal of Geophysical Research: Atmospheres*, *127*, e2022JD037434. https://doi.org/10.1029/2022JD037434

Received 2 JUL 2022
Accepted 17 OCT 2022

Author Contributions:

Conceptualization: Chunlei Gu, Anning Huang, Yaocun Zhang
Data curation: Chunlei Gu, Ben Yang, Shuxin Cai, Xiaoke Xu, Jiangxin Luo, Yang Wu
Formal analysis: Chunlei Gu, Yaocun Zhang, Ben Yang, Jiangxin Luo
Investigation: Chunlei Gu, Anning Huang, Yaocun Zhang, Ben Yang, Shuxin Cai, Xiaoke Xu
Methodology: Chunlei Gu, Anning Huang
Resources: Chunlei Gu, Yaocun Zhang, Xiaoke Xu, Yang Wu
Software: Chunlei Gu
Supervision: Anning Huang, Yaocun Zhang
Validation: Chunlei Gu, Anning Huang
Visualization: Chunlei Gu, Anning Huang, Shuxin Cai, Xiaoke Xu, Yang Wu
Writing – original draft: Chunlei Gu, Anning Huang

Abstract The Regional Climate Model Version 4 (RegCM4) with the conventional plane-parallel radiative transfer scheme severely overestimates the summer precipitation over the Tibetan Plateau (TP) due to the excessive surface heat source, which results from the poor representation of the sub-grid terrain-related radiation processes. To realistically describe the surface sub-grid radiation process in the RegCM4, a 3-dimensional sub-grid terrain solar radiative effect (3DSTSRE) parameterization scheme is implemented into the RegCM4 to improve the original plane-parallel radiative transfer scheme. Results show that adopting the 3DSTSRE scheme in RegCM4 can significantly reduce the summer (June–August) wet bias over the TP produced by the model with the plane-parallel radiative transfer scheme. Mechanism analysis indicates that the 3DSTSRE scheme largely improves the description of the TP surface energy balance in the RegCM4 by reducing the positive bias of downward surface solar radiation (DSSR). The reduced DSSR leads to the weakened surface heat source and cooler near-surface air over the TP. Consequently, the local atmospheric circulation adapts to the temperature field as the low-level anti-cyclonic (high-level cyclonic) anomaly over the TP. The adjustment of the temperature and wind field attenuates the water vapor transport, enhances the low-level atmospheric stability, inhibits the updraft motion, and eventually reduces the rainfall over TP. Although the 3DSTSRE improves the DSSR simulation only during daytime, the precipitation simulation is also improved at nighttime, which is fundamentally attributed to the maintenance of the cooled atmosphere throughout the daytime and nighttime.

1. Introduction

The Tibetan Plateau (TP) with elevated complex terrain remarkably influences the regional climate and water cycle (Duan et al., 2012; Wu et al., 2017; Zhong et al., 2019). However, the state of the art climate models generally have difficulty in reasonably reproducing the precipitation over TP (Mishra et al., 2019; Na et al., 2021; B. Yang et al., 2015). The global climate models of the Coupled Model Intercomparison Project Phase 5 (CMIP5) produce 62.0%~183.0% more rainfall than the observations over the TP (Mueller & Seneviratne, 2014; Su et al., 2013). The wet bias over the TP (WBT) remains in the CMIP6 (Cui et al., 2021; Zhu & Yang, 2020). Even the regional climate models (RCMs) with much higher horizontal resolution have similar WBT problem (Y. Gao et al., 2015; Guo et al., 2018).

Various factors cause the WBT problem of climate models, for example, the uncertainties in the initial conditions due to scarce observations over the TP (P. Zhao et al., 2018), the inappropriate description of TP cumulus characteristic (Kukulies et al., 2021; Y. Li & Zhang, 2017; W. Xu & Zipser, 2011), particularly the poor representation of the complex terrain-related processes in the models (Hu & Yuan, 2021; Sun et al., 2021), and so on. How to reduce the WBT over TP has become a hot issue and great efforts have been made to improve the precipitation simulation over the TP (Z. Liu et al., 2022; X. Wang et al., 2018). Driving the model with high-accuracy initial conditions, assimilating the observations, and adopting proper cumulus scheme all can improve the TP precipitation simulation to a certain degree (Park et al., 2013; X. Wang et al., 2021; Xie et al., 2021; B. Yang, Zhou, et al., 2018). Studies show that increasing the model horizontal resolution also effectively reduces the WBT (H. Gu, Yu, et al., 2020; Ji & Kang, 2013; Kan et al., 2015; Liang et al., 2021; Rahimi et al., 2019) because the simulated excessive water vapor transport (WVT) is suppressed by the increased model terrain height (Jain et al., 2019; Lin et al., 2018; Y. Zhao et al., 2021; Zhou et al., 2021). But the WBT still exists in the simulations with the model horizontal resolution of a few kilometers (P. Li, Furtado, Zhou, Chen, & Li, 2021).

Writing – review & editing: Anning Huang, Yaocun Zhang, Ben Yang, Shuxin Cai, Xiaoke Xu, Jiangxin Luo, Yang Wu

To improve the simulation of precipitation over the regions with complex terrains, increasing the level of detail in the description of the terrain-related physical processes is more important than increasing the model resolution alone (Dirmeyer et al., 2012). The turbulent orographic form drag scheme remains its added-value in reducing the WBT at the model resolution of 0.03° (Y. Wang et al., 2020). In addition, correctly representing the TP soil type can also restrain the WBT (Yue et al., 2021). Adopting the Community Land Model Version 4.5 (CLM4.5) with a greater level of detail in the sub-grid land surface processes in climate models can produce a decrease of WBT compared to the other land surface models adopted (H. Gu, Yu, et al., 2020; X. Wang et al., 2015).

The Regional Climate Model Version 4 (RegCM4) has been widely applied to the Earth science studies (Lu et al., 2021; Zou et al., 2013). No matter of the configurations of resolution, cover region, forcing data, and physical schemes, the RegCM4 often produces the WBT in summer (Chen et al., 2014; Giorgi et al., 2012; Oh et al., 2014; Park et al., 2013; X. Wang et al., 2021; M. Yang, Zuo, et al., 2018; S. Zhang et al., 2015). The RegCM4 provides a non-hydrostatic dynamic core lately, but the new core still cannot fix the WBT problem (Coppola et al., 2021; Nguyen-Xuan et al., 2022).

Although it is urgent to realistically describe the sub-grid terrain radiative effects (STRE) in climate models with the horizontal resolution increased, only a few climate models consider the STRE due to the lack of efficient STRE scheme (Y. Gu et al., 2012; Lee et al., 2011). Implementing a 2-dimensional STRE (2DSTRE) parameterization scheme into the RegCM4 improved the description of STRE and thereafter the simulation of the summer precipitation over China (C. Gu, Huang, et al., 2020). But the 2DSTRE scheme has native shortcomings from its overly idealized and simplified effect of sub-grid terrain (it only considers the effect of sub-grid terrain slope and aspect on the solar incident angle) on surface radiation (Kondrat'yev, 1965; Y. Zhang et al., 2006), for example, overestimation of the downward surface solar radiation (DSSR) during the period with low solar elevation angle. To completely consider the radiative effects of the 3-dimensional structure (i.e., terrain slope and aspect, terrain shading, and sky view factor, etc.) of sub-grid terrain (Dozier & Frew, 1990; X. Li et al., 2002), we have recently developed a 3-dimensional sub-grid terrain solar radiative effect (3DSTSRE) parameterization scheme to realistically describe the effect of sub-grid terrain on DSSR (A. Huang et al., 2022; X. Zhang et al., 2022). The 3DSTSRE scheme has been systematically tested in the Common Land Model (CoLM) and the results showed the ability of CoLM in simulating the land surface energy balance and hydrothermal status can be significantly improved by adopting the 3DSTSRE scheme (X. Zhang et al., 2022).

To further improve the performance of RegCM4 in simulating the summer precipitation over the TP, we coupled the 3DSTSRE scheme with RegCM4 and indicate how the scheme affects the performance of RegCM4 in simulating the summer precipitation over the TP. The underlying physical mechanisms are also deeply revealed. Findings of the study may provide a necessary base to further develop climate models and improve the precipitation simulation over the TP and surrounding regions with complex terrains.

Section 2 introduces the RegCM4, the 3DSTSRE scheme, data sets, and metrics. The effects of 3DSTSRE scheme on the performance of RegCM4 are evaluated in Section 3. Section 4 indicates the underlying physical mechanisms of the 3DSTSRE scheme affecting the simulated summer precipitation over TP. Section 5 gives the conclusion and discussion.

2. RCM, 3DSTSRE Scheme, Data and Methodology

2.1. Regional Climate Model

The RegCM is the first RCM around the world and originally developed by the National Center for Atmospheric Research (Dickinson et al., 1989; Giorgi, 1990). The RegCM has been developed and maintained by the Abdus Salam International Center for Theoretical Physics (ICTP) since the RegCM Version 3 (RegCM3, Pal et al., 2007). Compared to the RegCM3, the latest RegCM4 (available at https://github.com/ictp-esp/RegCM, Coppola et al., 2021) provides the additional non-hydrostatic dynamic core and abundant new choices of physical schemes that is, the Tiedtke cumulus scheme (Tiedtke, 1996), the Kain-Fritsch cumulus scheme (Kain, 2004; Kain & Fritsch, 1990), the University of Washington (UW) planetary boundary layer scheme (Bretherton et al., 2004), the CLM4.5 land surface model (Oleson et al., 2013), the Nogherotto-Tompkins explicit moisture scheme (Nogherotto et al., 2016), the Rapid Radiative Transfer Model (RRTMG, Mlawer et al., 1997), and so on.

Table 1
List of Symbols

Symbol	Meaning
a_p	The grid-scale surface albedo
C_{ad}	The adjustment parameter for grid-scale shading factor
DIRC_p	The grid-scale terrain correction factor for the downward direct solar radiation flux
DIFC_p	The grid-scale terrain correction factor for the downward diffuse solar radiation flux from the sky
dx	The model horizontal resolution in kilometers
E_{ac}	The solar constant
$E_{dir,p\downarrow}$	The plane-surface grid-scale downward direct solar radiation
$E_{dif,p\downarrow}$	The plane-surface grid-scale downward diffuse solar radiation
$E_{dirt,p\downarrow}$	The rugged surface grid-scale downward direct solar radiation
$E_{dift,p\downarrow}$	The rugged surface grid-scale downward diffuse solar radiation from the sky
$E_{reft,p\downarrow}$	The rugged surface grid-scale reflecting solar radiation from the surrounding terrain
$E_{dift,p\downarrow o2m}$	The final rugged surface grid-scale downward diffuse solar radiation
$E_{dirt,p\uparrow}$	The rugged surface grid-scale upward direct solar radiation
$E_{dift,p\uparrow}$	The rugged surface grid-scale upward diffuse solar radiation
I_p	The grid-scale solar incident angle
REFC_p	The grid-scale terrain correction factor for the reflecting solar radiation flux from the surrounding terrains
SECA_p	The area weight coefficient
SF_i	The sub-grid shading factor
$< \mathrm{SF}_i >_{i\rightarrow p}$	The grid-scale shading factor
SFC_p	The adjusted grid-scale shading factor
SVF_i	The sub-grid sky-view factor
TACB_p	The grid-scale factor A for the calculation of DIRC_p
TASB_p	The grid-scale factor B for the calculation of DIRC_p
Z_p	The grid-scale solar zenith angle
α_i	The sub-grid terrain slope
β_i	The sub-grid terrain aspect
θ_p	The grid-scale solar azimuth angle

2.2. The 3DSTSRE Parameterization Scheme

The 3DSTSRE parameterization scheme (A. Huang et al., 2022) is conducted mainly by two steps:

1. The grid-scale terrain correction factors for modifying the surface solar radiation (SSR) simulation of plane-parallel radiative scheme are first calculated from the sub-grid terrain parameters (i.e., terrain slope and aspect, sky view factor, shading factor, and the maximal terrain elevation angles along different directions, etc.) derived from the sub-grid terrain elevation data with high-resolution before the model run. The terrain correction factors are calculated by Equations 1–7. The variables α_i, β_i, SVF_i, and SF_i are the sub-grid terrain slope, aspect, sky-view factor, and shading factor respectively (the symbols are listed in Table 1). Their definitions and detailed calculation methods are introduced in A. Huang et al. (2022). The correction factors TACB_p, TASB_p, SECA_p, DIFC_p, and REFC_p (Figures 1a–1e) are only related to the sub-grid scale terrain and time-independent. The grid-scale shading factor $< \mathrm{SF}_i >_{i\rightarrow p}$ and adjusted grid-scale shading factor SFC_p (Figures 1f–1i) are dependent on both the sub-grid scale terrain and the time. Thus , $< \mathrm{SF}_i >_{i\rightarrow p}$ of each model grid is generated statistically under different combinations of 360 azimuth angles and 100 levels of the maximal terrain elevation angle along each azimuth by the method described in A. Huang et al. (2022) and X. Zhang et al. (2022). The adjustment parameter C_{ad} is the function of the model horizontal resolution dx (Equation 7). In this study, dx is 20 km and C_{ad} is 0.048.

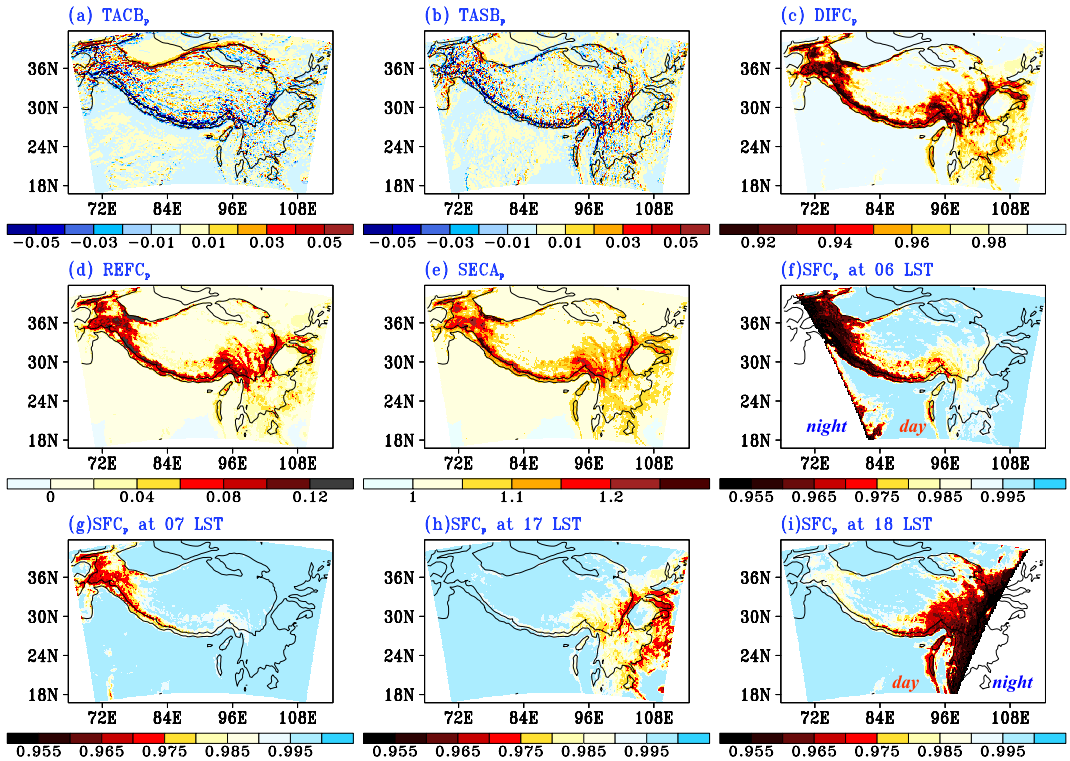

Figure 1. The terrain correction factors for the 3DSTSRE scheme in the model domain with a horizontal resolution of 20 km, $TACB_p$ (a), $TASB_p$ (b), $DIFC_p$ (c), $REFC_p$ (d), $SECA_p$ (e), the SFC_p at 06 LST (f), 07 LST (g), 17LST (h), and 18 LST (i) on 1 July 2010. The thin (thick) lines indicate the elevation of 1,000 m (3,000 m).

$$\mathrm{TACB}_p = \frac{1}{n}\sum_{i=1}^{i=n} \tan\alpha_i \cos\beta_i \tag{1}$$

$$\mathrm{TASB}_p = \frac{1}{n}\sum_{i=1}^{i=n} \tan\alpha_i \sin\beta_i \tag{2}$$

$$\mathrm{SECA}_p = \frac{1}{n}\sum_{i=1}^{i=n} \sec\alpha_i \tag{3}$$

$$\mathrm{DIFC}_p = \frac{1}{n}\sum_{i=1}^{i=n} \frac{\sec\alpha_i \cdot \mathrm{SVF}_i}{2}(1+\cos\alpha_i) \tag{4}$$

$$\mathrm{REFC}_p = \frac{1}{n}\sum_{i=1}^{i=n} \left(\frac{1+\cos\alpha_i}{2} - \mathrm{SVF}_i\right)\sec\alpha_i \tag{5}$$

$$\mathrm{SFC}_p = 1 - C_{ad}(1- < \mathrm{SF}_i >_{i\to p}) \tag{6}$$

$$C_{ad} = 0.1849 dx^{-1.443} + 0.04561 \tag{7}$$

Figure 1 shows the grid-scale terrain correction factors derived from the 3″ (~90 m) Shuttle Radar Topography Mission (SRTM) V4.1 digital elevation model data (Jarvis et al., 2008) in the model domain. The $TACB_p$, $TASB_p$, and SFC_p are the terrain correction factors for the direct solar radiation. The model grid with larger absolute value of $TACB_p$ ($TASB_p$) and smaller SFC_p has larger impacts of sub-grid terrain on the grid-scale direct solar radiation. Smaller $DIFC_p$ indicates that the sub-grid terrain makes less diffuse solar radiation reach the grid land surface. The grid with larger $REFC_p$ receives extra solar energy due to the reflecting solar radiation from the surrounding terrains. The grid with more complex sub-grid terrain has larger area weight factor $SECA_p$. From Figure 1, the most significant 3DSTSRE can be found along the western, southern, and southeastern flank of TP.

2. The SSR components of the RegCM4 model are modified by the above terrain correction factors during the model integration. According to Equations 8–11, the grid-scale rugged surface downward direct solar radiation $E_{dirt,p\downarrow}$, diffuse solar radiation $E_{dift,p\downarrow}$, and solar radiation reflecting from the surrounding terrains $E_{reft,p\downarrow}$ are calculated by the terrain correction factors (Equations 1–7) and the grid-scale variables from the original plane-parallel radiative transfer scheme in the model. The variables $E_{dir,p\downarrow}$, $E_{dif,p\downarrow}$, Z_p , θ_p , and a_p are the plane-surface downward direct solar radiation, the plane-surface downward diffuse solar radiation, the solar zenith, the solar azimuth, and the surface albedo at a given model grid, respectively. E_{ac} is the solar constant. Following the previous studies (Arnold et al., 2006; Senkova et al., 2007), the reflecting solar radiation ($E_{reft,p\downarrow}$) from the surrounding terrains is added to the rugged surface downward diffuse solar radiation ($E_{dift,p\downarrow}$), thus, $E_{dift,p\downarrow o2m}$ (Equation 12) is the final rugged surface downward diffuse solar radiation in the model. To maintain the energy balance, the rugged surface upward direct solar radiation $E_{dirt,p\uparrow}$ and diffuse solar radiation $E_{dift,p\uparrow}$ should be calculated by Equations 13 and 14. The cosine of grid-scale solar incident angle cos I_p is calculated by Equations 15 and 16 to determine whether it is daytime or nighttime at surface instead of cos Z_p (cos $I_p > 0.0$ is the daytime). Detailed information about the 3DSTSRE scheme are introduced in A. Huang et al. (2022).

$$E_{dirt,p\downarrow} = \max\left(\mathrm{SFC}_p \cdot \mathrm{DIRC}_p \frac{E_{dir,p\downarrow}}{\cos Z_p} / \mathrm{SECA}_p, 0.0\right) \tag{8}$$

$$\mathrm{DIRC}_p = \cos Z_p + \mathrm{TACB}_p \sin Z_p \cos\theta_p + \mathrm{TASB}_p \sin Z_p \sin\theta_p \tag{9}$$

$$E_{dift,p\downarrow} = \begin{cases} E_{dif,p\downarrow}\left[\dfrac{E_{dirt,p\downarrow}}{E_{ac}} + \mathrm{DIFC}_p\left(1 - \dfrac{E_{dir,p\downarrow}}{E_{ac}}\right)/\mathrm{SECA}_p\right], \text{if}\,\mathrm{DIRC}_p > 0 \\ E_{dif,p\downarrow}\left[\mathrm{DIFC}_p\left(1 - \dfrac{E_{dir,p\downarrow}}{E_{ac}}\right)/\mathrm{SECA}_p\right], \text{otherwise} \end{cases} \tag{10}$$

$$E_{reft,p\downarrow} = (E_{dir,p\downarrow} + E_{dif,p\downarrow})\, a_p \mathrm{REFC}_p / \mathrm{SECA}_p \tag{11}$$

$$E_{dift,p\downarrow o2m} = E_{dift,p\downarrow} + E_{reft,p\downarrow} \tag{12}$$

$$E_{dirt,p\uparrow} = E_{dirt,p\downarrow} \cdot \left(a_p + \frac{E_{dir,p\downarrow} - E_{dirt,p\downarrow}}{E_{dirt,p\downarrow}}\right) \tag{13}$$

$$E_{dift,p\uparrow} = E_{dift,p\downarrow o2m} \cdot \left(a_p + \frac{E_{dif,p\downarrow} - E_{dift,p\downarrow o2m}}{E_{dift,p\downarrow o2m}}\right) \tag{14}$$

$$\cos I_p = u_p \cos Z_p + v_p \sin Z_p \cos\theta_p + w_p \sin Z_p \sin\theta_p \tag{15}$$

$$\begin{cases} u_p = \dfrac{1}{n}\sum_{i=1}^{i=n} \cos\alpha_i \\ v_p = \dfrac{1}{n}\sum_{i=1}^{i=n} \sin\alpha_i \cos\beta_i \\ w_p = \dfrac{1}{n}\sum_{i=1}^{i=n} \sin\alpha_i \sin\beta_i \end{cases} \tag{16}$$

2.3. Numerical Experimental Design

Two numerical experiments driven by the same initial and lateral conditions have been carried out in this study. The experiment by the RegCM4 with (without) the 3DSTSRE scheme is called SEXP (CTRL) experiment. Following Ou et al. (2020) and X. Wang et al. (2016), the domain centered at 30°N, 90°E with 210 (132) grids in the east-west (north-south) direction at the horizontal resolution of 20 km covers the TP and its surrounding region (Figure 2). Since the grid-scale topography derived from the SRTM data is quite consistent with the RegCM4 default grid-scale topography (not shown), this study adopts the default grid-scale topography, which is provided by the United States Geological Survey (USGS) Global Multi-resolution Terrain Elevation Data (GMTED, Danielson & Gesch, 2011) with a resolution of 30″. The simulation is run by the MM5 hydrostatical core (Grell et al., 1994) with 18 vertical levels of atmosphere and 50 hPa at the model top.

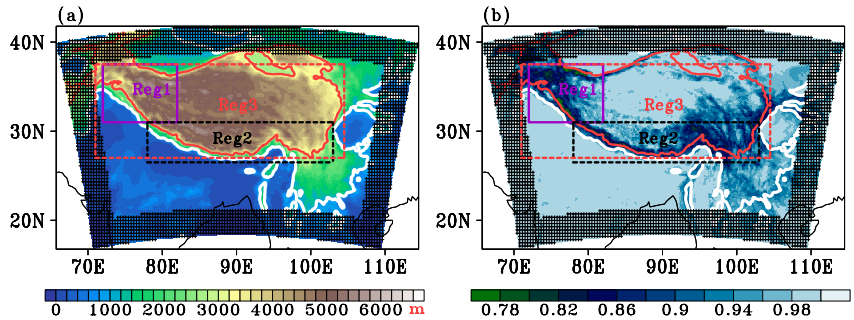

Figure 2. Grid-scale terrain elevation (a) and sky-view factor (b) in the model domain with a horizontal resolution of 20 km. The white (red) solid lines indicate the terrain elevation of 1,000 m (3,000 m). The Reg1 (Reg2, Reg3) is the region above 3,000 m (1,000, 3,000 m) in the purple (black-dash, red-dash) rectangle. The black girds indicate the lateral buffer zone.

Following H. Gu, Yu, et al. (2020), the physical package used in this study are the CLM4.5 land surface model (Oleson et al., 2013), the Tiedtke cumulus scheme (Tiedtke, 1996), the Holtslag planetary boundary layer scheme (Holtslag et al., 1990), the SUBgrid EXplicit moisture scheme (Pal et al., 2000), the Zeng ocean flux scheme (Zeng et al., 1998), and the CCM3 Column Radiation Model (Kiehl et al., 1998).

The weekly National Oceanic and Atmospheric Administration (NOAA) Optimum Interpolation Sea Surface Temperature with a resolution of 1° (Reynolds et al., 2002) provides the oceanic surface condition. The initial and boundary conditions are derived from the 6 hourly European Center for Medium Range Weather Forecasts (ECMWF) ERA-Interim reanalysis with a horizontal resolution of 0.75° at 37 vertical levels (Dee et al., 2011). The lateral boundary condition adopts the relaxation exponential technique with the boundary width of 18 grids (the black grids in Figure 2). The soil moisture is initialized by the European Space Agency Climate Change Initiative Essential Climate Variable (ESA CCI ECV) Surface Soil Moisture Combined Product (Y. Y. Liu et al., 2012) averaged from 1979 to 2013, which greatly saves the model spin-up time (Bisselink et al., 2011).

The model time step is 30 s. The solar radiation module, the absorption-emission module, the land surface model, and the cumulus module are called with the interval of 10 min, 1 hr, 10, and 2 min, respectively. The model integration for each experiment starts at 00:00 UTC on 1 May and ends at 00:00 UTC on 1 September in each year of 2010–2014. The model output interval is 1 hr. The first month of simulation in each year is taken as the spin-up time following X. Gao et al. (2016), Kang et al. (2014), and Koné et al. (2022), so the simulations of each experiment during June to August in each year of 2010–2014 are used for analysis. The differences between SEXP and CTRL simulations indicate the impacts of the 3DSTSRE scheme on the performance of RegCM4 model.

2.4. Data for Model Evaluation

In this study, we have used the data for model evaluation as follows:

1. The half hourly Integrated Multi-satellitE Retrievals for Global Precipitation Measurement (GPM) Final Precipitation L3 (Huffman et al., 2019) with a resolution of 0.1° from 00:00 UTC 1 June to 23:30 UTC 31 August in each year of 2010–2014. The GPM data are in reasonable agreement with the ground observations (Ma et al., 2016; R. Xu et al., 2017) and widely used in the studies of precipitation over the TP (Lai et al., 2021; G. Li, Yu, Wang, Ju, & Chen, 2021; Tang et al., 2018).
2. The monthly surface incoming shortwave radiation (SIS) from the EUMETSAT CM SAF Cloud, Albedo, Radiation data set, AVHRR-based, Edition 2.1 (CLARA-A2.1) Surface Radiation Products (Karlsson et al., 2020) with a resolution of 0.25° from June to August in each year of 2010–2014.
3. The hourly Fifth generation of the ECWMF atmospheric reanalyses (ERA5, Hersbach et al., 2020) with a horizontal resolution of 0.25° from 00:00 UTC on 1 June to 23:00 UTC on 31 August in each year of 2010–2014.

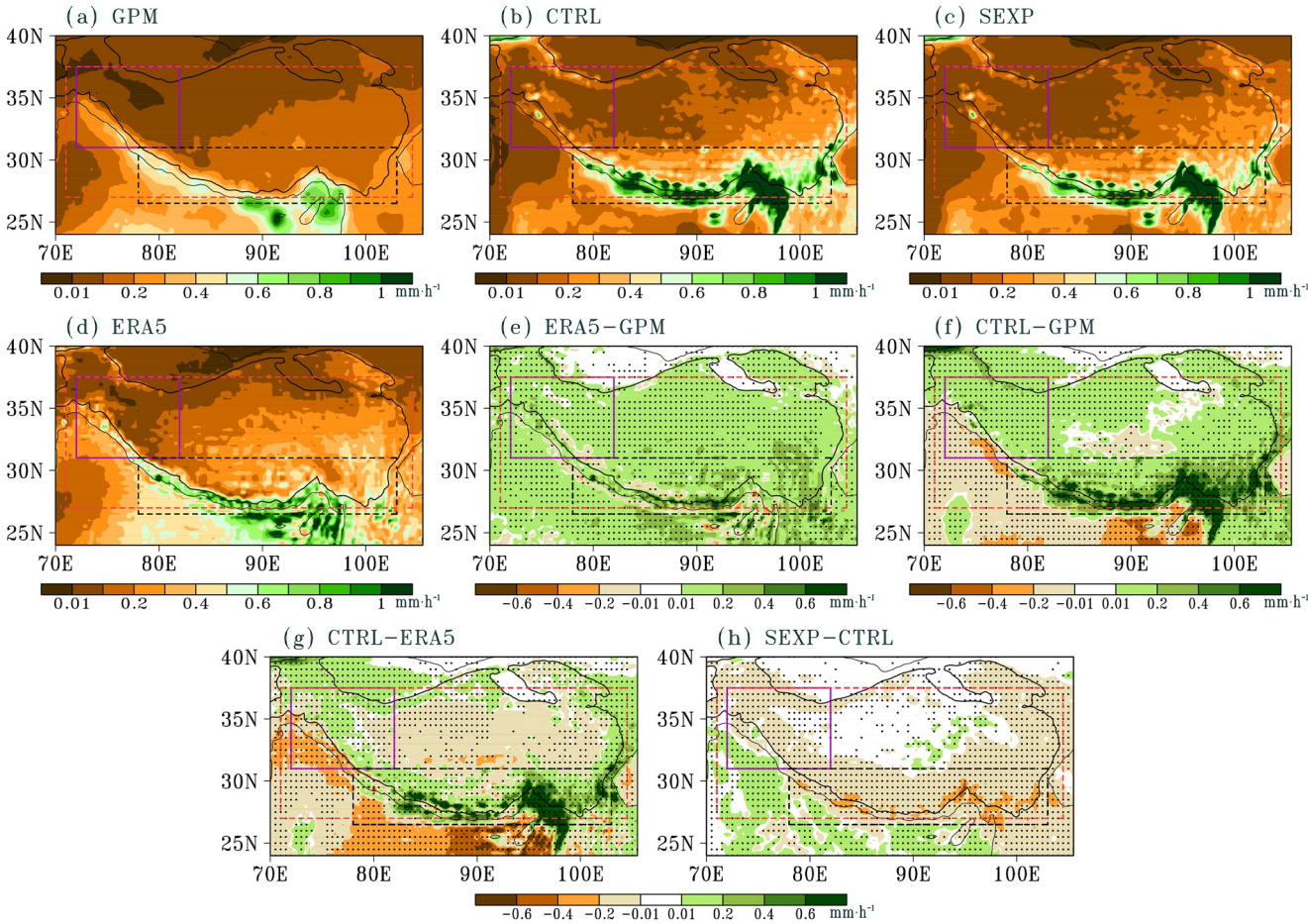

Figure 3. The summer mean precipitation from Global Precipitation Measurement (GPM) (a), simulations of the CTRL (b) and SEXP (c) experiments, and ERA5 (d) averaged over 2010–2014. The summer precipitation differences between the ERA5 data and the GPM data (e), between the CTRL experiment and the GPM data (f), between the CTRL experiment and the ERA5 data (g), and between the SEXP and CTRL experiments (h). The thin (thick) black lines indicate the elevation of 1,000 m (3,000 m). The Reg1 (Reg2, Reg3) is the region above 3,000 m (1,000, 3,000 m) in the purple (black-dash, red-dash) rectangle. The black dots in panels (e–h) indicate the significant level above 95% of *t*.

2.5. Methodology

Following Tian et al. (2015) and Yu et al. (2010), the accumulated precipitation with an hourly precipitation greater than 0.1 mm·h^{-1} during the daytime (nighttime) is divided by the total hours during the daytime (nighttime) to obtain the daytime (nighttime) precipitation.

The Taylor score (TS, Taylor, 2001) and root mean square error (RMSE) are used for quantitative evaluation of the simulated precipitation. TS is a comprehensive score of the magnitude and pattern variability (Taylor, 2001). TS varies from 0.0 to 1.0 and larger TS indicates higher skill. Smaller value of RMSE indicates the simulation with lower biases. The Student's *t* -test (Owen, 1965) is used to test the significance of the differences in Figures 3, 4, 8, 10, and 11.

The grid-scale sky-view factor (Figure 2b) is derived from the 3″(~90 m) sub-grid sky-view factor. The smaller the grid-scale sky-view factor is, the stronger the 3DSTSRE is. Three sub-regions for model evaluation are selected according to the magnitude of 3DSTSRE and climate regime. The Reg1 and Reg2 are two sub-regions with the most significant 3DSTSRE but with different climate. The Reg1 is the arid region in western TP (Zheng et al., 2013) above 3,000 m (shown in Figure 2 with purple solid-line rectangle, 72°~82°E, 31°~37.5°N) with the WVT mainly from the westerlies (Ma et al., 2018). The Reg2 mostly affected by the WVT from the Indian summer monsoon (B. Huang et al., 2015; Ma et al., 2020) covers the southern TP with the terrain height above 1,000 m (shown in Figure 2 with black dash-line rectangle, 78°~103°E, 26.5°~31°N). Previous studies

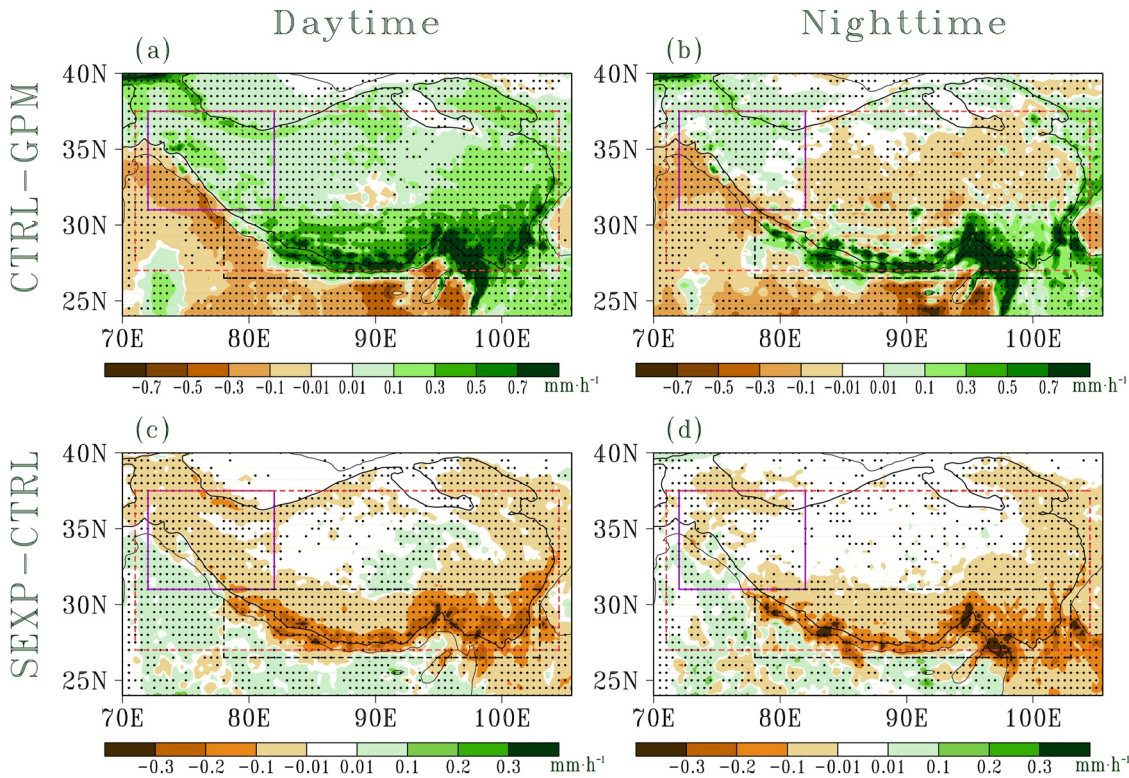

Figure 4. The daytime and nighttime precipitation differences between the CTRL experiment and the Global Precipitation Measurement (GPM) data (a, b), and between the SEXP experiment and the CTRL experiment (c, d) in summer averaged over 2010–2014. The thin (thick) black lines indicate the elevation of 1,000 m (3,000 m). The Reg1 (Reg2, Reg3) is the region above 3,000 m (1,000, 3,000 m) in the purple (black-dash, red-dash) rectangle. The black dots indicate the significant level above 95% of *t* test.

have shown that the largest wet bias over TP is located in Reg2 (Cui et al., 2021; Xin et al., 2020). The Reg3 with the terrain height above 3,000 m covers most area of TP (shown in Figure 2 with red dash-line rectangle, 71°∼104.5°E, 27°∼37.5°N).

3. Model Evaluation

Both GPM and ERA5 data show very similar spatial distribution of precipitation (Figures 3a and 3d). As shown in Figure 3b, compared to the GPM and ERA5 data (Figures 3a and 3d), the CTRL experiment adopting the RegCM4 without the 3DSTSRE scheme can well reproduce the overall spatial distribution characteristic of the summer precipitation decreasing from southeast to northwest over the TP. However, the CTRL experiment tends to overestimate the precipitation over most TP especially in the regions with complex terrain (Figures 3f and 3g). The SEXP experiment with the adoption of 3DSTSRE scheme clearly reduces the overestimation of summer precipitation over the TP especially Reg2 with complex terrain in the CTRL experiment to a considerable degree (Figure 3h).

Figure 4a shows that the RegCM4 overestimates the daytime precipitation over most TP in the CTRL experiment. During nighttime, the precipitation in the CTRL experiment shows weak negative biases (∼0.1 mm·h^{-1}) over most of the TP but strong positive biases along the TP edges with complex terrains (Figure 4b). The largest biases of the daytime and nighttime precipitation in the CTRL experiment are all located in the south edge of TP with much more complex terrain, especially the region with the elevation from 1,000 to 3,000 m (>0.7 mm·h^{-1}, Figures 4a and 4b). The differences of the daytime and nighttime precipitation between the SEXP and CTRL experiments are within ±0.1 mm·h^{-1} over most of the TP (Figures 4c and 4d). The largest differences of daytime and nighttime precipitation between the SEXP and CTRL experiments are also located over the south edge of TP with the values exceeding −0.3 mm·h^{-1}.

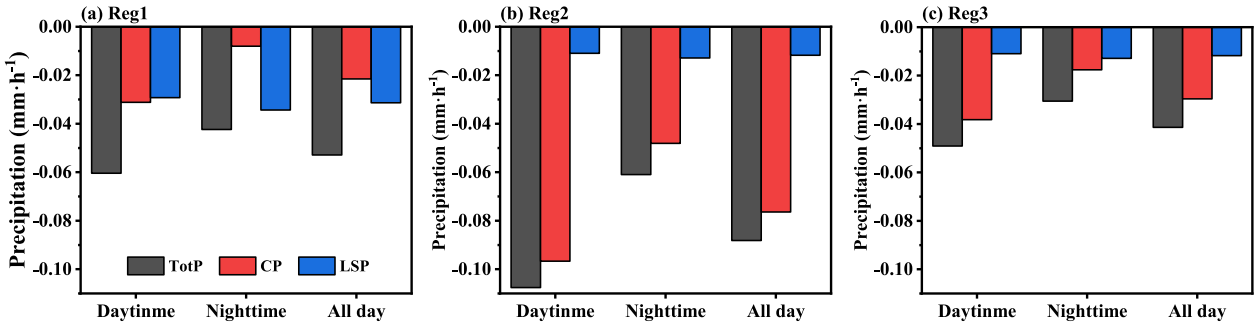

Figure 5. The differences of the simulated summer total precipitation (TotP), convective precipitation (CP), and large-scale precipitation (LSP) during daytime, nighttime, and all day averaged over 2010–2014 in the three sub-regions (Figure 2) between the SEXP and CTRL.

The regional mean total precipitation (TotP), convective precipitation (CP), and large-scale precipitation (LSP) in the SEXP experiment all decrease compared to those in the CTRL experiment during both daytime and nighttime over the each sub-region (Figure 5). The decrease of the overestimated TotP induced by adopting the 3DSTSRE scheme mainly comes from the reduced LSP (CP) over the Reg1 (Reg2 and Reg3; Figures 5a–5c).

Compared to the CTRL experiment, the SEXP experiment produces much lower RMSE (higher TS) of the modeled precipitation against the GPM observation over each sub-region at most hours of a day (Figure 6), indicating that adopting the 3DSTSRE scheme in RegCM4 can effectively improve the precipitation simulation at most time of a day. To further investigate the general performance of the 3DSTSRE scheme, the RMSE (TS) of the daytime mean, nighttime mean, and all-day mean precipitation produced by the CTRL and SEXP experiments are also calculated (Figure 7), which also confirms the improved precipitation simulation with the adoption of the 3DSTSRE scheme. It is interesting that although the 3DSTSRE scheme modifies the simulated SSR only during daytime, the simulated precipitation can also be improved at nighttime (Figures 4, 6, and 7).

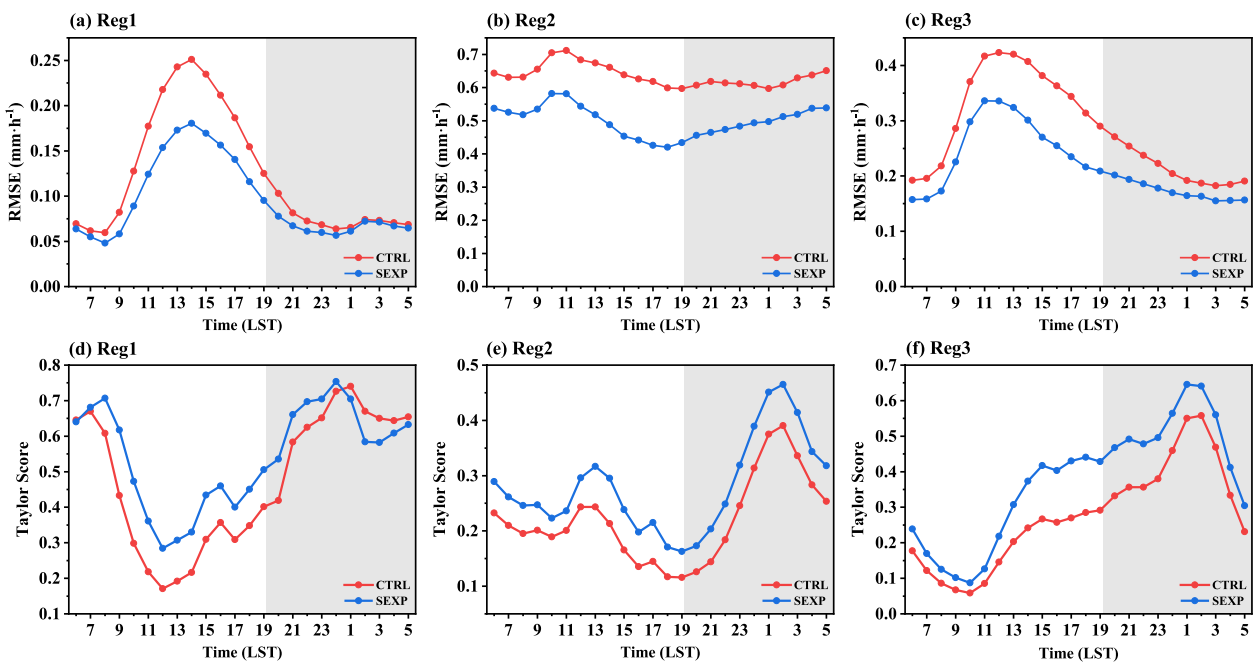

Figure 6. The root mean square error (RMSE) (a–c) and TS (d–f) of the hourly simulated summer precipitation averaged over 2010–2014 in the three sub-regions (Figure 2) from the CTRL and SEXP experiments against the Global Precipitation Measurement (GPM) data. The gray background shows the nighttime.

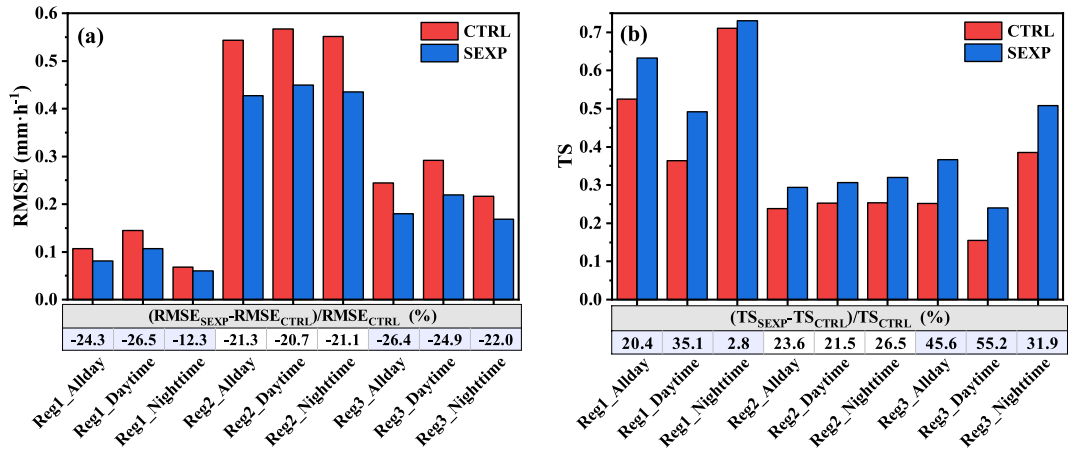

Figure 7. The root mean square error (RMSE) (a) and TS (b) of the simulated summer precipitation averaged over 2010–2014 in the three sub-regions (Figure 2) from the CTRL and SEXP experiments during all day, daytime, and nighttime against the Global Precipitation Measurement (GPM) data. Tables show the relative changes of the RMSE and TS produced by the SEXP experiment compared to the CTRL experiment.

4. Physical Mechanism

The CLARA data indicate the DSSR fluxes over TP increase from southeast to northwest (Figure 8a), which is opposite to the rainfall distribution (Figure 3). In the CTRL experiment, the RegCM4 without the 3DSTSRE captures the main features of the DSSR distribution (Figure 8b) but overestimates the DSSR more than 30 $W \cdot m^{-2}$ in most TP (Figure 8d). The simulated DSSR fluxes in the SEXP experiment decrease more than 10 $W \cdot m^{-2}$ over southeastern TP and more than 30 $W \cdot m^{-2}$ over the southern and western TP compared to the CTRL experiment (Figure 8e), which clearly reduce the positive biases of DSSR fluxes over most TP simulated by the CTRL experiment (Figures 8d and 8e).

As shown in Figure 9a, regarding the CLARA data as the "true value" and compared to CTRL experiment, the RMSEs of the DSSR fluxes in the SEXP experiment considering the 3DSTSRE can be reduced by 34.7%, 24.8%, and 17.4% over the Reg1, Reg2, and Reg3, respectively. The 3DSTSRE scheme clearly improves the description of DSSR in the RegCM4 over the complex terrains. Consequently, the overestimation of surface heat fluxes in the CTRL experiment are obviously reduced (not shown). Compared to the CTRL experiment, the SEXP experiment with the 3DSTSRE scheme improves the simulation of surface turbulent heat fluxes, whose RMSE in daytime (nighttime) against the ERA5 data is reduced by 31.0% (9.1%) over Reg1, 35.0% (6.9%) over Reg2, and 26.8% (5.0%) over Reg3 (Figure 9b).

Figure 10 shows the differences of the wind (temperature) between the CTRL experiment and ERA5 data, and between the SEXP and CTRL experiments at 500 and 200 hPa. During the daytime, compared to the ERA5 data, the CTRL experiments shows positive temperature anomalies accompanied with the cyclonic (anti-cyclonic) wind anomalies at 500 hPa (200 hPa), suggesting that the RegCM4 overestimates the near-surface cyclone and South Asia High above the TP (Figures 10a and 10c). The increase of daytime temperature at 500 hPa is stronger than that at 200 hPa over the Reg1, which makes the air column more unstable and promotes the upward motion in the CTRL experiment. The daytime wind differences between the CTRL experiment and ERA5 data are convergent (divergent) at 500 (200) hPa over the Reg2, which also promotes the updrafts. The SEXP experiment shows negative temperature anomalies accompanied with the anti-cyclonic (cyclonic) wind anomalies at 500 hPa (200 hPa) compared to the CTRL experiment, suggesting that the 3DSTSRE attenuates the simulated near-surface cyclone and South Asia High above the TP (Figures 10e and 10g). The decrease of daytime temperature at 500 hPa is stronger than that at 200 hPa over the Reg1, which makes the air column more stable and inhibits the upward motion in the SEXP experiment. The daytime wind differences between the SEXP and CTRL experiments are divergent (convergent) at 500 (200) hPa over the Reg2, which also inhibits the updrafts. The differences of the temperature (wind) between the CTRL experiment and the ERA5 data during the nighttime are similar to those during the daytime (Figures 10b and 10d). Although the 3DSTSRE scheme impacts the simulated DSSR only during the daytime, the differences of the wind (temperature) between the SEXP and CTRL experiments during

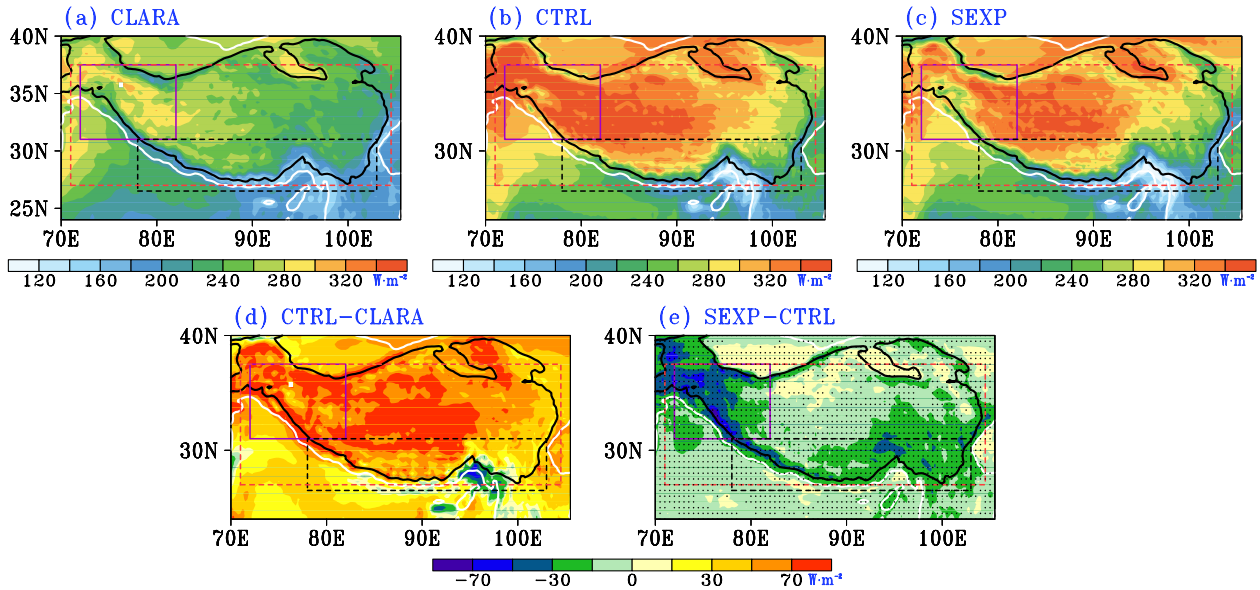

Figure 8. The summer mean DSSR from the CLARA data sets (a) and the simulations of the CTRL (b) and SEXP (c) experiments averaged over 2010–2014. The summer mean downward surface solar radiation (DSSR) differences between the CTRL experiment and the CLARA data (d), and between the SEXP and CTRL (e). The white (black) lines indicate the elevation of 1,000 m (3,000 m). The Reg1 (Reg2, Reg3) is the region above 3,000 m (1,000, 3,000 m) in the purple (black-dash, red-dash) rectangle. The black dots in Figure 6e indicate the significant confidence level above 95% of *t* test.

the nighttime resembles those during the daytime (Figures 10f and 10h). The sustained day-night atmospheric changes (vitally the cooled atmosphere) resulted from the 3DSTSRE in the SEXP experiment are fundamental to the improvement of precipitation simulation throughout the day.

Figures 11a–11d show that the CTRL experiment can reproduce the general characteristics of the summer WVT over the TP and its surrounding area during both daytime and nighttime. However, the CTRL experiment

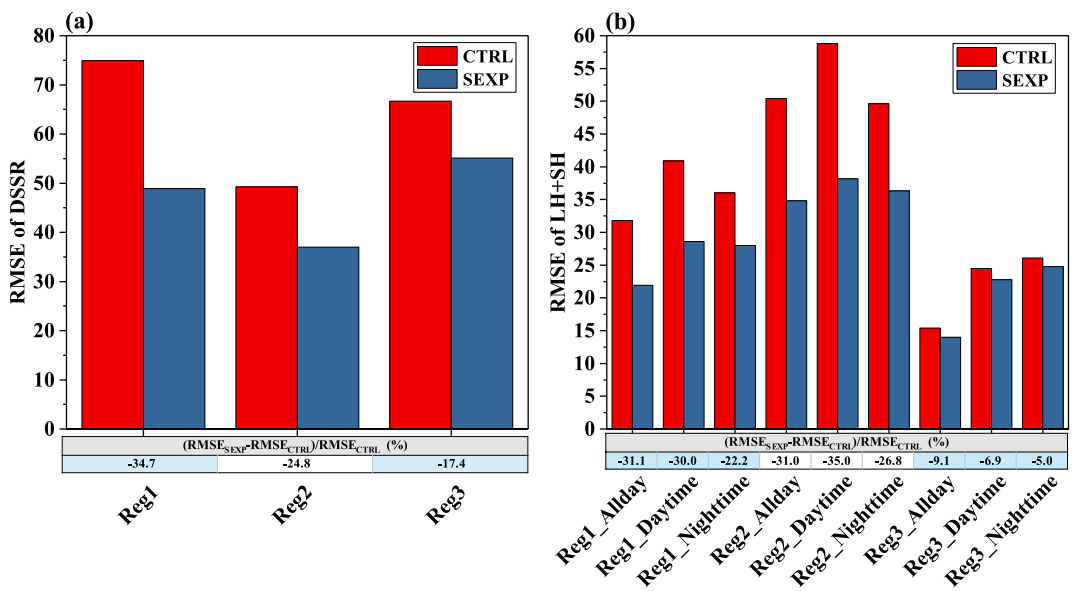

Figure 9. The root mean square error (RMSE) of modeled summer mean downward surface solar radiation (DSSR) during daytime against the CLARA data (a) and modeled summer mean total surface latent and sensible heat fluxes against the ERA5 data during all day, daytime, and nighttime (b) averaged over 2010–2014 in each sub-region (Figure 2). Tables show the relative changes of the root mean square error (RMSE) produced by the SEXP experiment compared to the CTRL experiment.

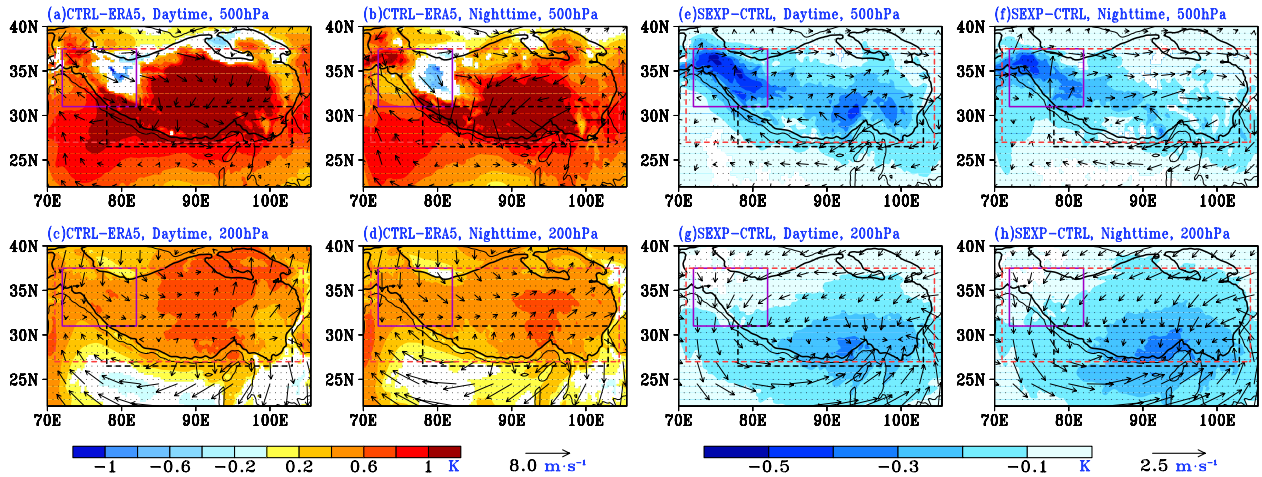

Figure 10. The differences of summer mean temperature (shaded) and wind (vector) simulations between the CTRL experiment and the ERA5 data (a–d) and between the SEXP and CTRL (e–h) at 500 hPa (a–b, e–f) and 200 hPa (c–d, g–h) during daytime and nighttime averaged over 2010–2014. The thin (thick) black lines indicate the elevation of 1,000 m (3,000 m). The Reg1 (Reg2, Reg3) is the region above 3,000 m (1,000, 3,000 m) in the purple (black-dash, red-dash) rectangle. The black dots indicate the wind differences passing the significant level of 95% of *t* test. The temperature differences shown with colors pass the significant level of 95% of *t* test.

overestimated the southern-southwestern WVT over the TP edges (Figures 11e and 11f). Figures 11g and 11h show that the SEXP experiment with the 3DSTSRE can clearly reduce the overestimation of the WVT over the southern and western TP in the CTRL experiment, which is directly related to the atmospheric circulation adjustment (anti-cyclonic wind anomalies over the TP and divergent wind anomalies over the southern TP at 500 hPa, Figure 10). The wind anomalies are the adaptions to the cooled atmosphere (Figure 10) resulted from the reduced DSSR (Figure 8) and thereafter decreased surface heat flux, which is the consequence of the better representation of the surface energy balance (Figure 9) due to the adoption of the 3DSTSRE scheme. The excessively simulated WVT is a vital reason for the rainfall overestimation over the TP in the CTRL experiment. In the previous studies (Y. Wang et al., 2020; Zhou et al., 2019), the overestimation of the simulated WVT and rainfall over the TP edges (such as Pamir and Himalayas) are mainly attributed to the unrealistically smoothed terrain and thereby weakened terrain drag in the models. According to the results in this study, the lack of the description of 3DSTSRE in the models is also an important cause of the overestimated WVT and precipitation over the TP.

To further present the changes of the simulated atmospheric state due to the 3DSTSRE, Figure 12 illustrates the profiles of the regionally averaged differences of pseudo-equivalent potential temperature (θ_{se}) and the vertical speed (ω) between the SEXP and CTRL experiments. According to the profiles of the regionally averaged θ_{se} anomalies (Figures 12a and 12b), the air columns in the SEXP experiment over the three sub-regions, especially the Reg1, are much more stable than that in the CTRL experiment (Saucier, 1955). Figures 12c and 12d show that the upward motions are weakened in the SEXP experiment over all the sub-regions terrifically over the Reg2 with much more complex terrain compared to the CTRL experiment, this is consistent with the divergent (convergent) wind anomalies at 500 (200) hPa over the Reg2 (Figure 10). Overall, the 3DSTSRE makes the RegCM4 reproduce more stable atmosphere with weaker upward motions over the TP, leading to the overestimated precipitation in the CTRL experiment largely reduced at both daytime and nighttime.

5. Conclusion and Discussion

The 3DSTSRE parameterization scheme is implemented in the RegCM4 to correct the calculations of original plane-parallel radiative transfer scheme. The impacts of the 3DSTSRE scheme on the performance of the RegCM4 in simulating the summer precipitation over the TP during 2010–2014 are discussed in this study. The main conclusions are listed as follows:

1. The RegCM4 with the original plane-parallel radiative transfer scheme can reproduce the overall spatial distribution features of the summer precipitation over the TP but significantly overestimates the precipitation. The overestimated precipitation can in a large part be attributed to the excessively simulated surface heat source over the TP, which is largely due to the deficient description of the sub-grid terrain-related processes.

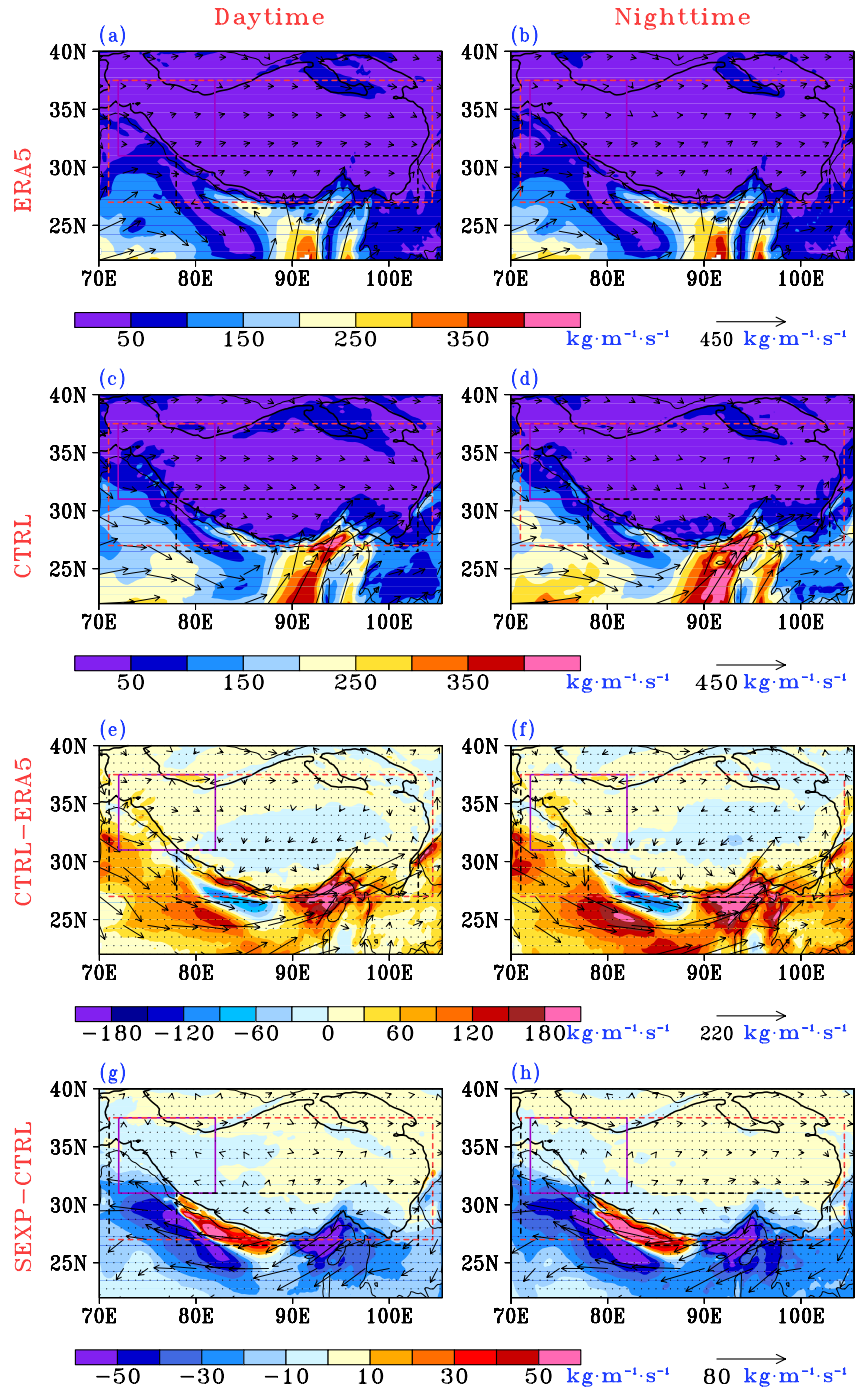

Figure 11. The summer mean vertical integral (surface to 100 hPa) of the water vapor flux from ERA5 (a, b) and simulations of the CTRL experiment (c, d) averaged over 2010–2014. The summer vertical integral of the water vapor flux differences between the CTRL experiment and the ERA5 data (e, f), and between the SEXP and CTRL experiments (g, h) during daytime and nighttime. The thin (thick) black lines indicate the elevation of 1,000 m (3,000 m). The Reg1 (Reg2, Reg3) is the region above 3,000 m (1,000, 3,000 m) in the purple (black-dash, red-dash) rectangle. The black dots in panels (e–h) indicate the significant level above 95% of *t* test.

Compared to the CLARA data, the original RegCM4 overestimates the regionally averaged DSSR fluxes over the TP with considerable RMSE.

2. The 3DSTSRE scheme offers the RegCM4 a better description of the surface energy balance and reduces the RMSE of simulated DSSR by more than 17.4%, 34.7%, and 24.8% over the TP, the western TP, and the

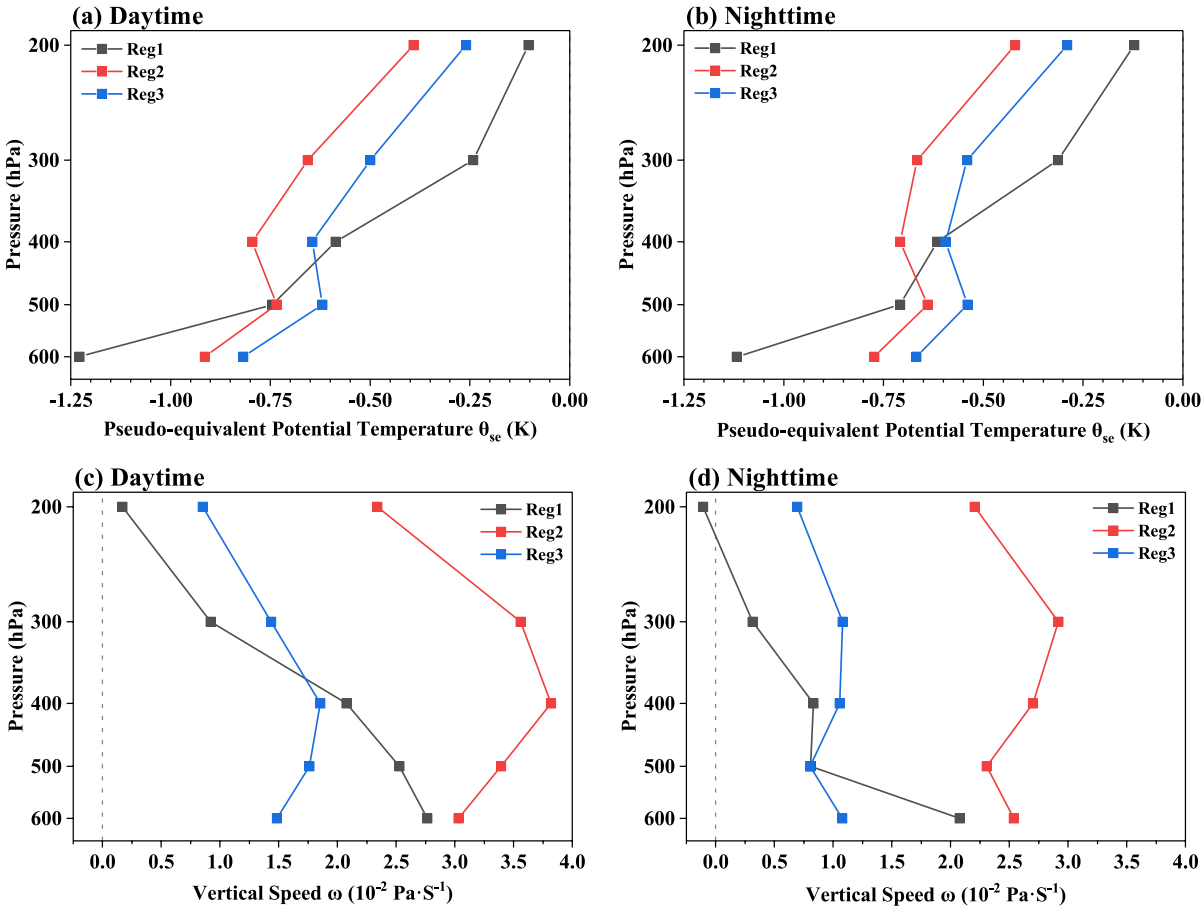

Figure 12. Differences of the regionally averaged summer mean pseudo-equivalent potential temperature (a, b) and vertical speed (c, d) between the SEXP experiment and CTRL experiment during daytime and nighttime averaged over 2010–2014 in each sub-region shown in Figure 2.

southern TP, respectively. The reduction of the simulated DSSR leads to the weakened surface heat source and cooler near-surface air over the TP. Thereafter, the local atmospheric circulation adapts to the atmospheric temperature field as the low-level anti-cyclonic (high-level cyclonic) differences over the TP. The adjustment of the temperature and wind field attenuates the WVT, enhances the atmospheric stability, inhibits the updrafts, and finally reduces the rainfall over the TP.

3. Compared to the original RegCM4, the RegCM4 with the 3DSTSRE scheme significantly decreases the overestimated precipitation over the TP in summer with the TS in daytime (nighttime) increased by 55.2% (31.9%) and the RMSE in daytime (nighttime) precipitation decreased by 24.9% (22.0%), respectively. Although the 3DSTSRE improves the DSSR simulation only during daytime, the simulated precipitation is also improved at both daytime and nighttime, this is fundamentally attributed to the maintenance of the cooled atmosphere throughout the day.

However, the 3DSTSRE scheme does not totally solve the WBT problem. The WBT problem is also blamed to the insufficient description of the sub-grid scale dynamic processes (i.e., the gravity wave drag, GWD and the turbulent orographic formed drag, TOFD) in the models (Zhou et al., 2017). The abilities to represent the sub-grid GWD or TOFD differ a lot among the RCMs. The Regional Climate-Weather Research and Forecasting Model (CWRF) accounts for both the sub-grid GWD and TOFD (Liang et al., 2012). The consortium for small-scale modeling (COSMO) regional climate model (COSMO-CLM) and HIRHAM regional climate model only include the parameterization of GWD (Dosio & Panitz, 2016; Rinke et al., 1999). The sub-grid GWD and TOFD are not revealed in the official version of RegCM4. We recently have coupled the TOFD scheme to the RegCM4. We are now investigating the impacts of the TOFD scheme on the performance of the RegCM4 over the East Asia and will report the results in the near future.

Although encouraging findings are uncovered in this study, we have to admit that this study is only a primary assessment of the performance of the 3DSTSRE scheme and has its limitations (i.e., findings relative to a specific area, specific horizontal resolution, and limited to the simulation of only five summers, only 18 vertical levels and hydrostatical core adopted in the RegCM4 model, etc). Therefore, more in-depth studies should be carried out and reported in the future to fully understand the mechanisms of the 3DSTSRE scheme influencing the climatic modeling, such as further analysis of different areas (e.g., Alps and Rocky Mountains), with long-term simulation period, in different seasons, at different time-scales, and investigation of extreme events.

Data Availability Statement

Data used in this study are listed as follows: the Global Multi-resolution Terrain Elevation Data (GMTED, Danielson & Gesch, 2011, available at https://pubs.er.usgs.gov/publication/ofr20111073), the Shuttle Radar Topography Mission (SRTM) 90 m Digital Elevation Database v4.1 (Jarvis et al., 2008, https://developers.google.com/earth-engine/datasets/catalog/CGIAR_SRTM90_V4), the weekly National Oceanic and Atmospheric Administration (NOAA) Optimum Interpolation Sea Surface Temperature with a resolution of 1° (Reynolds et al., 2002, available at https://psl.noaa.gov/data/gridded/data.noaa.oisst.v2.html), the fifth generation of ECWMF atmospheric reanalyses (Hersbach et al., 2020, available at https://www.ecmwf.int/en/forecasts/datasets/reanalysis-datasets/era5), the European Space Agency Climate Change Initiative Essential Climate Variable (ESA CCI ECV) Surface Soil Moisture Combined Product (Y. Y. Liu et al., 2012, available at https://esa-soilmoisture-cci.org/v06.1_release), the Integrated Multi-satellitE Retrievals for Global Precipitation Measurement (IMERG) Final Precipitation L3 (Huffman et al., 2019, available at https://doi.org/10.5067/GPM/IMERG/3B-HH/06), the European Centre for Medium Range Weather Forecasts (ECMWF) ERA-Interim reanalysis (Dee et al., 2011) which is available at https://www.ecmwf.int/en/forecasts/datasets/reanalysis-datasets/era-interim, and the EUMETSAT CM SAF Cloud, Albedo, Radiation data set, AVHRR-based, Edition 2.1 (CLARA-A2.1) Surface Radiation Products (Karlsson et al., 2020) which is available at https://doi.org/10.5676/EUM_SAF_CM/CLARA_AVHRR/V002_01). The source codes of Regional Climate Model 4 (RegCM4) used in this study is available at https://doi.org/10.5281/zenodo.7161718. The source codes for calculations of sub-grid scale terrain elements, the grid scale 3DSTSRE modification factors, and the revised RegCM4 codes with the 3DSTSRE scheme are available at https://doi.org/10.5281/zenodo.7161213.

Acknowledgments

This study is the National Natural Science Foundation of China under Grant 41975081, the CAS "Light of West China" Program (E12903010, Y929641001), the Research Funds for the Frontiers Science Center for Critical Earth Material Cycling Nanjing University, the Fundamental Research Funds for the Central Universities (020914380103), the Jiangsu University "Blue Project" outstanding young teachers training object, and the Jiangsu Collaborative Innovation Center for Climate Change. The authors are grateful to ICTP for its open source policy (https://github.com/ictp-esp/RegCM) and allowing us to use RegCM4. The authors appreciate CIAT, ECWMF, NOAA, USGS, ESA, NASA, and EUMETSAT for allowing us to use their data set. The authors show our deepest respect and warm appreciation to the three anonymous reviewers for their constructive suggestions to greatly improve the manuscript.

References

Arnold, N. S., Rees, W. G., Hodson, A. J., & Kohler, J. (2006). Topographic controls on the surface energy balance of a high Arctic valley glacier. *Journal of Geophysical Research: Earth Surface*, *111*(F2). https://doi.org/10.1029/2005jf000426

Bisselink, B., van Meijgaard, E., Dolman, A. J., & de Jeu, R. A. M. (2011). Initializing a regional climate model with satellite-derived soil moisture. *Journal of Geophysical Research: Atmospheres*, *116*(D2). https://doi.org/10.1029/2010JD014534

Bretherton, C. S., McCaa, J. R., & Grenier, H. (2004). A new parameterization for shallow cumulus convection and its application to marine subtropical cloud-topped boundary layers. Part I: Description and 1D results. *Monthly Weather Review*, *132*(4), 864–882. https://doi.org/10.1175/1520-0493(2004)132<0864:anpfsc>2.0.co;2;2

Chen, J., Yin, Y., Chen, Q., Ding, H., & Xiao, H. (2014). Effect of convection schemes on the simulation of monsoon climates: A sensitivity study using RegCM4. *Climate Research*, *60*(2), 147–162. https://doi.org/10.3354/cr01229

Coppola, E., Stocchi, P., Pichelli, E., Torres Alavez, J. A., Glazer, R., Giuliani, G., et al. (2021). Non-hydrostatic RegCM4 (RegCM4-NH): Model description and case studies over multiple domains. *Geoscientific Model Development*, *14*(12), 7705–7723. https://doi.org/10.5194/gmd-14-7705-2021

Cui, T., Li, C., & Tian, F. (2021). Evaluation of temperature and precipitation simulations in CMIP6 models over the Tibetan Plateau. *Earth and Space Science*, *8*(7), e2020EA001620. https://doi.org/10.1029/2020EA001620

Danielson, J. J., Gesch, D. B. (2011). Global multi-resolution terrain elevation data 2010 (GMTED2010): *US Geological Survey Open-File Report* 2011–1073. https://doi.org/10.3133/ofr20111073

Dee, D. P., Uppala, S. M., Simmons, A. J., Berrisford, P., Poli, P., Kobayashi, S., et al. (2011). The ERA-Interim reanalysis: Configuration and performance of the data assimilation system. *Quarterly Journal of the Royal Meteorological Society*, *137*(656), 553–597. https://doi.org/10.1002/qj.828

Dickinson, R. E., Errico, R. M., Giorgi, F., & Bates, G. T. (1989). A regional climate model for the western United States. *Climatic Change*, *15*(3), 383–422. https://doi.org/10.1007/BF00240465

Dirmeyer, P. A., Cash, B. A., Kinter, J. L., Jung, T., Marx, L., Satoh, M., et al. (2012). Simulating the diurnal cycle of rainfall in global climate models: Resolution vs. parameterization. *Climate Dynamics*, *39*(1), 399–418. https://doi.org/10.1007/s00382-011-1127-9

Dosio, A., & Panitz, H. J. (2016). Climate change projections for CORDEX-Africa with COSMO-CLM regional climate model and differences with the driving global climate model. *Climate Dynamics*, *46*(5), 1599–1625. https://doi.org/10.1007/s00382-015-2664-4

Dozier, J., & Frew, J. (1990). Rapid calculation of terrain parameters for radiation modeling from digital elevation data. *IEEE Transactions on Geoscience and Remote Sensing*, *28*(5), 963–969. https://doi.org/10.1109/36.58986

Duan, A., Wu, G., Liu, Y., Ma, Y., & Zhao, P. (2012). Weather and climate effects of the Tibetan Plateau. *Advances in Atmospheric Sciences*, *29*(5), 978–992. https://doi.org/10.1007/s00376-012-1220-y

Gao, X., Shi, Y., & Giorgi, F. (2016). Comparison of convective parameterizations in RegCM4 experiments over China with CLM as the land surface model. *Atmospheric and Oceanic Science Letters*, *9*(4), 246–254. https://doi.org/10.1080/16742834.2016.1172938

Gao, Y., Xu, J., & Chen, D. (2015). Evaluation of WRF mesoscale climate simulations over the Tibetan Plateau during 1979–2011. *Journal of Climate*, *28*(7), 2823–2841. https://doi.org/10.1175/jcli-d-14-00300.1

Giorgi, F. (1990). Simulation of regional climate using a limited area model nested in a general circulation model. *Journal of Climate*, *3*(9), 941–963. https://doi.org/10.1175/1520-0442(1990)003<0941:sorcua>2.0.co;2;2

Giorgi, F., Coppola, E., Solmon, F., Mariotti, L., Sylla, M., Bi, X., et al. (2012). RegCM4: Model description and preliminary tests over multiple CORDEX domains. *Climate Research*, *52*, 7–29. https://doi.org/10.3354/cr01018

Grell, G. A., Dudhia, J., & Stauffer, D. R. (1994). Description of the fifth generation Penn State/NCAR Mesoscale Model (MM5). Tech. Rep. TN-398+STR, NCAR.

Gu, C., Huang, A., Wu, Y., Yang, B., Mu, X., Zhang, X., & Cai, S. (2020). Effects of subgrid terrain radiative forcing on the ability of RegCM4.1 in the simulation of summer precipitation over China. *Journal of Geophysical Research: Atmospheres*, *125*(12), e2019JD032215. https://doi.org/10.1029/2019JD032215

Gu, H., Yu, Z., Peltier, W., & Wang, X. (2020). Sensitivity studies and comprehensive evaluation of RegCM4.6.1 high-resolution climate simulations over the Tibetan Plateau. *Climate Dynamics*, *54*(7), 3781–3801. https://doi.org/10.1007/s00382-020-05205-6

Gu, Y., Liou, K., Lee, W., & Leung, L. (2012). Simulating 3-D radiative transfer effects over the Sierra Nevada Mountains using WRF. *Atmospheric Chemistry and Physics*, *12*(20), 9965–9976. https://doi.org/10.5194/acp-12-9965-2012

Guo, D., Sun, J., & Yu, E. (2018). Evaluation of CORDEX regional climate models in simulating temperature and precipitation over the Tibetan Plateau. *Atmospheric and Oceanic Science Letters*, *11*(3), 219–227. https://doi.org/10.1080/16742834.2018.1451725

Hersbach, H., Bell, B., Berrisford, P., Hirahara, S., Horányi, A., Muñoz-Sabater, J., et al. (2020). The ERA5 global reanalysis. *Quarterly Journal of the Royal Meteorological Society*, *146*(730), 1999–2049. https://doi.org/10.1002/qj.3803

Holtslag, A. A. M., De Bruijn, E. I. F., & Pan, H. L. (1990). A high resolution air mass transformation model for short-range weather forecasting. *Monthly Weather Review*, *118*(8), 1561–1575. https://doi.org/10.1175/1520-0493(1990)118<1561:ahramt>2.0.co;2;2

Hu, X., & Yuan, W. (2021). Evaluation of ERA5 precipitation over the eastern periphery of the Tibetan Plateau from the perspective of regional rainfall events. *International Journal of Climatology*, *41*(4), 2625–2637. https://doi.org/10.1002/joc.6980

Huang, A., Gu, C., Zhang, Y., Li, W., Zhang, J., Wu, Y., et al. (2022). Development of a clear-sky 3D sub-grid terrain solar radiative effect parameterization scheme based on the mountain radiation theory. *Journal of Geophysical Research: Atmospheres*, *127*, e2022JD036449. https://doi.org/10.1029/2022JD036449

Huang, B., Polanski, S., & Cubasch, U. (2015). The assessment of precipitation climatology in an ensemble of CORDEX-East Asia regional climate simulations. *Climate Research*, *64*(2), 141–158. https://doi.org/10.3354/cr01302

Huffman, G. J., Stocker, E. F., Bolvin, D. T., Nelkin, E. J., & Tan, J. (2019). GPM IMERG final precipitation L3 half hourly 0.1° × 0.1° V06 [Dataset]. Goddard Earth Sciences Data and Information Services Center (GES DISC). https://doi.org/10.5067/GPM/IMERG/3B-HH/06

Jain, S., Mishra, S. K., Salunke, P., & Sahany, S. (2019). Importance of the resolution of surface topography vis-à-vis atmospheric and surface processes in the simulation of the climate of Himalaya-Tibet highland. *Climate Dynamics*, *52*(7), 4735–4748. https://doi.org/10.1007/s00382-018-4411-0

Jarvis, A., Reuter, H. I., Nelson, A., & Guevara, E. (2008). The Shuttle Radar Topography Mission (SRTM) 90 m Digital Elevation Database v4.1 [Dataset]. International Centre for Tropical Agriculture (CIAT). Retrieved from https://developers.google.com/earth-engine/datasets/catalog/CGIAR_SRTM90_V4

Ji, Z., & Kang, S. (2013). Double-nested dynamical downscaling experiments over the Tibetan Plateau and their projection of climate change under two RCP scenarios. *Journal of the Atmospheric Sciences*, *70*, 1278–1290. https://doi.org/10.1175/JAS-D-12-0155.1

Kain, J. S. (2004). The Kain-Fritsch convective parameterization: An update. *Journal of Applied Meteorology*, *43*(1), 170–181. https://doi.org/10.1175/1520-0450(2004)043<0170:tkcpau>2.0.co;2;2

Kain, J. S., & Fritsch, J. M. (1990). A one-dimensional entraining/detraining plume model and its application in convective parameterization. *Journal of the Atmospheric Sciences*, *47*, 2784–2802. https://doi.org/10.1175/1520-0469(1990)047<2784:aodepm>2.0.co;2

Kan, M., Huang, A., Zhao, Y., Zhou, Y., Yang, B., & Wu, H. (2015). Evaluation of the summer precipitation over China simulated by BCC-CSM model with different horizontal resolutions during the recent half-century. *Journal of Geophysical Research: Atmospheres*, *120*, 4657–4670. https://doi.org/10.1002/2015JD023131

Kang, S., Im, E. S., & Ahn, J. B. (2014). The impact of two land-surface schemes on the characteristics of summer precipitation over East Asia from the RegCM4 simulations. *International Journal of Climatology*, *34*(15), 3986–3997. https://doi.org/10.1002/joc.3998

Karlsson, K.-G., Anttila, K., Trentmann, J., Stengel, M., Solodovnik, I., Meirink, J., et al. (2020). CLARA-A2.1: CM SAF cLoud, Albedo and surface RAdiation data set from AVHRR data - Edition 2.1 [Dataset]. Satellite Application Facility on Climate Monitoring. https://doi.org/10.5676/EUM_SAF_CM/CLARA_AVHRR/V002_01

Kiehl, J. T., Hack, J. J., Bonan, G. B., Boville, B. A., Williamson, D. L., & Rasch, P. J. (1998). The National Center for Atmospheric Research Community Climate Model: CCM3. *Journal of Climate*, *11*(6), 1131–1149. https://doi.org/10.1175/1520-0442(1998)011<1131:tncfar>2.0.co;2;2

Kondrat'yev, K. Y. (1965). *Radiative heat exchange in the atmosphere* (p. 332). Pergamon Press. (Translated from the Russian by O. Tedder). https://doi.org/10.1016/C2013-0-05325-X

Koné, B., Diedhiou, A., Diawara, A., Anquetin, S., Touré, N. E., Bamba, A., & Kobea, A. T. (2022). Influence of initial soil moisture in a regional climate model study over West Africa—Part 1: Impact on the climate mean. *Hydrology and Earth System Sciences*, *26*(3), 711–730. https://doi.org/10.5194/hess-26-711-2022

Kukulies, J., Chen, D., & Curio, J. (2021). The role of mesoscale convective systems in precipitation in the Tibetan Plateau region. *Journal of Geophysical Research: Atmospheres*, *126*(23), e2021JD035279. https://doi.org/10.1029/2021JD035279

Lai, H. W., Chen, H. W., Kukulies, J., Ou, T., & Chen, D. (2021). Regionalization of seasonal precipitation over the Tibetan Plateau and associated large-scale atmospheric systems. *Journal of Climate*, *34*(7), 2635–2651. https://doi.org/10.1175/jcli-d-20-0521.1

Lee, W. L., Liou, K. N., & Hall, A. (2011). Parameterization of solar fluxes over mountain surfaces for application to climate models. *Journal of Geophysical Research: Atmospheres*, *116*(D1). https://doi.org/10.1029/2010jd014722

Li, G., Yu, Z., Wang, W., Ju, Q., & Chen, X. (2021). Analysis of the spatial distribution of precipitation and topography with GPM data in the Tibetan Plateau. *Atmospheric Research*, *247*, 105259. https://doi.org/10.1016/j.atmosres.2020.105259

Li, P., Furtado, K., Zhou, T., Chen, H., & Li, J. (2021). Convection-permitting modeling improves simulated precipitation over the central and eastern Tibetan Plateau. *Quarterly Journal of the Royal Meteorological Society*, *147*(734), 341–362. https://doi.org/10.1002/qj.3921

Li, X., Koike, T., & Cheng, G. (2002). Retrieval of snow reflectance from Landsat data in rugged terrain. *Annals of Glaciology*, *34*, 31–37. https://doi.org/10.3189/172756402781817635

Li, Y., & Zhang, M. (2017). The role of shallow convection over the Tibetan Plateau. *Journal of Climate*, *30*(15), 5791–5803. https://doi.org/10.1175/jcli-d-16-0599.1

Liang, X., Xu, M., Yuan, X., Ling, T., Choi, H., Zhang, F., et al. (2012). Regional climate-weather research and forecasting model. *Bulletin of the American Meteorological Society*, *93*(9), 1363–1387. https://doi.org/10.1175/bams-d-11-00180.1

Liang, Y., Yang, B., Wang, M., Tang, J., Sakaguchi, K., Leung, L. R., & Xu, X. (2021). Multiscale simulation of precipitation over East Asia by variable resolution CAM-MPAS. *Journal of Advances in Modeling Earth Systems*, *13*(11), e2021MS002656. https://doi.org/10.1029/2021MS002656

Lin, C., Chen, D., Yang, K., & Ou, T. (2018). Impact of model resolution on simulating the water vapor transport through the central Himalayas: Implication for models' wet bias over the Tibetan Plateau. *Climate Dynamics*, *51*(9), 3195–3207. https://doi.org/10.1007/s00382-018-4074-x

Liu, Y. Y., Dorigo, W. A., Parinussa, R. M., de Jeu, R. A. M., Wagner, W., McCabe, M. F., et al. (2012). Trend-preserving blending of passive and active microwave soil moisture retrievals. *Remote Sensing of Environment*, *123*, 280–297. https://doi.org/10.1016/j.rse.2012.03.014

Liu, Z., Gao, Y., & Zhang, G. (2022). How well can a convection-permitting-modeling improve the simulation of summer precipitation diurnal cycle over the Tibetan Plateau? *Climate Dynamics*, *58*(11–12), 1–18. https://doi.org/10.1007/s00382-021-06090-3

Lu, C., Huang, G., Wang, G., Zhang, J., Wang, X., & Song, T. (2021). Long-term projection of water cycle changes over China using RegCM. *Remote Sensing*, *13*(19), 3832. https://doi.org/10.3390/rs13193832

Ma, Y., Lu, M., Bracken, C., & Chen, H. (2020). Spatially coherent clusters of summer precipitation extremes in the Tibetan Plateau: Where is the moisture from? *Atmospheric Research*, *237*, 104841. https://doi.org/10.1016/j.atmosres.2020.104841

Ma, Y., Lu, M., Chen, H., Pan, M., & Hong, Y. (2018). Atmospheric moisture transport vs. precipitation across the Tibetan Plateau: A mini-review and current challenges. *Atmospheric Research*, *209*, 50–58. https://doi.org/10.1016/j.atmosres.2018.03.015

Ma, Y., Tang, G., Long, D., Yong, B., Zhong, L., Wan, W., & Hong, Y. (2016). Similarity and error intercomparison of the GPM and its predecessor-TRMM multisatellite precipitation analysis using the best available hourly gauge network over the Tibetan Plateau. *Remote Sensing*, *8*(7), 569. https://doi.org/10.3390/rs8070569

Mishra, S. K., Jain, S., Salunke, P., & Sahany, S. (2019). Past and future climate change over the Himalaya-Tibetan highland: Inferences from APHRODITE and NEX-GDDP data. *Climatic Change*, *156*(3), 315–322. https://doi.org/10.1007/s10584-019-02473-y

Mlawer, E. J., Taubman, S. J., Brown, P. D., Iacono, M. J., & Clough, S. A. (1997). Radiative transfer for inhomogeneous atmospheres: RRTM, a validated correlated-k model for the longwave. *Journal of Geophysical Research: Atmospheres*, *102*(D14), 16663–16682. https://doi.org/10.1029/97JD00237

Mueller, B., & Seneviratne, S. I. (2014). Systematic land climate and evapotranspiration biases in CMIP5 simulations. *Geophysical Research Letters*, *41*(1), 128–134. https://doi.org/10.1002/2013GL058055

Na, Y., Lu, R., Fu, Q., & Kodama, C. (2021). Precipitation characteristics and future changes over the southern slope of Tibetan Plateau simulated by a high-resolution global nonhydrostatic model. *Journal of Geophysical Research: Atmospheres*, *126*(3), e2020JD033630. https://doi.org/10.1029/2020JD033630

Nguyen-Xuan, T., Lam, S. L., Giorgi, F., Coppola, E., Giuliani, G., Gao, X., & Im, E.-S. (2022). Evaluation of the performance of the non-hydrostatic RegCM4 (RegCM4-NH) over southeastern China. *Climate Dynamics*, *58*(5), 1419–1437. https://doi.org/10.1007/s00382-021-05969-5

Nogherotto, R., Tompkins, A. M., Giuliani, G., Coppola, E., & Giorgi, F. (2016). Numerical framework and performance of the new multiple-phase cloud microphysics scheme in RegCM4.5: Precipitation, cloud microphysics, and cloud radiative effects. *Geoscientific Model Development*, *9*(7), 2533–2547. https://doi.org/10.5194/gmd-9-2533-2016

Oh, S.-G., Park, J. H., Lee, S.-H., & Suh, M.-S. (2014). Assessment of the RegCM4 over East Asia and future precipitation change adapted to the RCP scenarios. *Journal of Geophysical Research: Atmospheres*, *119*, 2913–2927. https://doi.org/10.1002/2013JD020693

Oleson, K. W., Lawrence, D. M., Bonan, G. B., Drewniak, B., Huang, M., Koven, C. D., et al. (2013). *Technical description of version 4.5 of the community land model (CLM)*. National Center for Atmospheric Research.NCAR technical note NCAR/TN-503 + STR.

Ou, T., Chen, D., Chen, X., Lin, C., Yang, K., Lai, H.-W., & Zhang, F. (2020). Simulation of summer precipitation diurnal cycles over the Tibetan Plateau at the gray-zone grid spacing for cumulus parameterization. *Climate Dynamics*, *54*(7), 3525–3539. https://doi.org/10.1007/s00382-020-05181-x

Owen, D. B. (1965). The Power of Student's *t* test. *Journal of the American Statistical Association*, *60*(309), 320–333. https://doi.org/10.1080/01621459.1965.10480794

Pal, J. S., Giorgi, F., Bi, X., Elguindi, N., Solmon, F., Gao, X., et al. (2007). Regional climate modeling for the developing world: The ICTP RegCM3 and RegCNET. *Bulletin of the American Meteorological Society*, *88*(9), 1395–1410. https://doi.org/10.1175/bams-88-9-1395

Pal, J. S., Small, E. E., & Eltahir, E. A. B. (2000). Simulation of regional-scale water and energy budgets: Representation of subgrid cloud and precipitation processes within RegCM. *Journal of Geophysical Research: Atmospheres*, *105*(D24), 29579–29594. https://doi.org/10.1029/2000JD900415

Park, J. H., Oh, S. G., & Suh, M. S. (2013). Impacts of boundary conditions on the precipitation simulation of RegCM4 in the CORDEX East Asia domain. *Journal of Geophysical Research: Atmospheres*, *118*(4), 1652–1667. https://doi.org/10.1002/jgrd.50159

Rahimi, S. R., Wu, C., Liu, X., & Brown, H. (2019). Exploring a variable-resolution approach for simulating regional climate over the Tibetan Plateau using VR-CESM. *Journal of Geophysical Research: Atmospheres*, *124*(8), 4490–4513. https://doi.org/10.1029/2018JD028925

Reynolds, R. W., Rayner, N. A., Smith, T. M., Stokes, D. C., & Wang, W. (2002). An improved in situ and satellite SST analysis for climate. *Journal of Climate*, *15*(13), 1609–1625. https://doi.org/10.1175/1520-0442(2002)015<1609:aiisas>2.0.co;2;2

Rinke, A., Dethloff, K., Spekat, A., Enke, W., & Christensen, J. H. (1999). High-resolution climate simulations over the Arctic. *Polar Research*, *18*(2), 143–150. https://doi.org/10.1111/j.1751-8369.1999.tb00286.x

Saucier, W. J. (1955). *Principles of meteorological analysis* (Vol. 438, pp. 76–78). University of Chicago Press.

Senkova, A. V., Rontu, L., & Savijarvi, H. (2007). Parametrization of orographic effects on surface radiation in HIRLAM. *Tellus*, *59*(3), 279–291. https://doi.org/10.1111/j.1600-0870.2007.00235.x

Su, F., Duan, X., Chen, D., Hao, Z., & Cuo, L. (2013). Evaluation of the global climate models in the CMIP5 over the Tibetan Plateau. *Journal of Climate*, *26*(10), 3187–3208. https://doi.org/10.1175/jcli-d-12-00321.1

Sun, G., Hu, Z., Ma, Y., Xie, Z., Sun, F., Wang, J., & Yang, S. (2021). Analysis of local land atmosphere coupling characteristics over Tibetan Plateau in the dry and rainy seasons using observational data and ERA5. *Science of the Total Environment*, *774*, 145138. https://doi.org/10.1016/j.scitotenv.2021.145138

Tang, G., Long, D., Hong, Y., Gao, J., & Wan, W. (2018). Documentation of multifactorial relationships between precipitation and topography of the Tibetan Plateau using spaceborne precipitation radars. *Remote Sensing of Environment*, *208*, 82–96. https://doi.org/10.1016/j.rse.2018.02.007

Taylor, K. E. (2001). Summarizing multiple aspects of model performance in a single diagram. *Journal of Geophysical Research*, *106*(D7), 7183–7192. https://doi.org/10.1029/2000JD900719

Tian, F., Zheng, Y., Zhang, T., Zhang, X., Mao, D., Sun, J., & Zhao, S. (2015). Statistical characteristics of environmental parameters for warm season short-duration heavy rainfall over central and eastern China. *Journal of Meteorological Research*, *29*(3), 370–384. https://doi.org/10.1007/s13351-014-4119-y

Tiedtke, M. (1996). An extension of cloud-radiation parameterization in the ECMWF model: The representation of subgrid-scale variations of optical depth. *Monthly Weather Review*, *124*(4), 745–750. https://doi.org/10.1175/1520-0493(1996)124<0745:aeocrp>2.0.co;2;2

Wang, X., Chen, D., Pang, G., Anwar, S. A., Ou, T., & Yang, M. (2021). Effects of cumulus parameterization and land-surface hydrology schemes on Tibetan Plateau climate simulation during the wet season: Insights from the RegCM4 model. *Climate Dynamics*, *57*(7), 1853–1879. https://doi.org/10.1007/s00382-021-05781-1

Wang, X., Pang, G., & Yang, M. (2018). Precipitation over the Tibetan Plateau during recent decades: A review based on observations and simulations. *International Journal of Climatology*, *38*(3), 1116–1131. https://doi.org/10.1002/joc.5246

Wang, X., Pang, G., Yang, M., & Wan, G. (2016). Effects of modified soil water-heat physics on RegCM4 simulations of climate over the Tibetan Plateau. *Journal of Geophysical Research: Atmospheres*, *121*(12), 6692–6712. https://doi.org/10.1002/2015JD024407

Wang, X., Yang, M., & Pang, G. (2015). Influences of two land-surface schemes on RegCM4 precipitation simulations over the Tibetan Plateau. *Advances in Meteorology*, *2015*, 106891. https://doi.org/10.1155/2015/106891

Wang, Y., Yang, K., Zhou, X., Chen, D. L., Lu, H., Ouyang, L., et al. (2020). Synergy of orographic drag parameterization and high resolution greatly reduces biases of WRF-simulated precipitation in central Himalaya. *Climate Dynamics*, *54*(3–4), 1729–1740. https://doi.org/10.1007/s00382-019-05080-w

Wu, G. X., He, B., Duan, A. M., Liu, Y. M., & Yu, W. (2017). Formation and variation of the atmospheric heat source over the Tibetan Plateau and its climate effects. *Advances in Atmospheric Sciences*, *34*(10), 1169–1184. https://doi.org/10.1007/s00376-017-7014-5

Xie, Q., Yang, Y., Qiu, X., Ma, Y., Lai, A., Lin, E., & Mai, X. (2021). 3D-var assimilation of GTS observation with the gravity wave drag scheme improves summer high-resolution climate simulation over the Tibetan Plateau. *Climate Dynamics*, *57*(1), 469–487. https://doi.org/10.1007/s00382-021-05720-0

Xin, X., Wu, T., Zhang, J., Yao, J., & Fang, Y. (2020). Comparison of CMIP6 and CMIP5 simulations of precipitation in China and the East Asian summer monsoon. *International Journal of Climatology*. https://doi.org/10.1002/joc.6590

Xu, R., Tian, F., Yang, L., Hu, H., Lu, H., & Hou, A. (2017). Ground validation of GPM IMERG and TRMM 3B42V7 rainfall products over southern Tibetan Plateau based on a high-density rain gauge network. *Journal of Geophysical Research: Atmospheres*, *122*(2), 910–924. https://doi.org/10.1002/2016JD025418

Xu, W., & Zipser, E. J. (2011). Diurnal variations of precipitation, deep convection, and lightning over and east of the eastern Tibetan Plateau. *Journal of Climate*, *24*(2), 448–465. https://doi.org/10.1175/2010jcli3719.1

Yang, B., Zhang, Y., Qian, Y., Huang, A., & Yan, H. (2015). Calibration of a convective parameterization scheme in the WRF model and its impact on the simulation of East Asian summer monsoon precipitation. *Climate Dynamics*, *44*(5–6), 1661–1684. https://doi.org/10.1007/s00382-014-2118-4

Yang, B., Zhou, Y., Zhang, Y., Huang, A., Qian, Y., & Zhang, L. (2018). Simulated precipitation diurnal cycles over East Asia using different CAPE-based convective closure schemes in WRF model. *Climate Dynamics*, *50*(5–6), 1639–1658. https://doi.org/10.1007/s00382-017-3712-z

Yang, M., Zuo, R., Wang, L., & Chen, X. (2018). Simulation of land surface climate over China with RegCM4.5: Verification and analysis. *Advances in Meteorology*, *2018*, 7960908. https://doi.org/10.1155/2018/7960908

Yu, R., Li, J., Yuan, W., & Chen, H. (2010). Changes in characteristics of late-summer precipitation over eastern China in the past 40 yr revealed by hourly precipitation data. *Journal of Climate*, *23*(12), 3390–3396. https://doi.org/10.1175/2010jcli3454.1

Yue, S., Yang, K., Lu, H., Zhou, X., Chen, D., & Guo, W. (2021). Representation of stony surface-atmosphere interactions in WRF reduces cold and wet biases for the southern Tibetan Plateau. *Journal of Geophysical Research: Atmospheres*, *126*(21). https://doi.org/10.1029/2021JD035291

Zeng, X., Zhao, M., & Dickinson, R. E. (1998). Intercomparison of bulk aerodynamic algorithms for the computation of sea surface fluxes using TOGA COARE and TAO data. *Journal of Climate*, *11*(10), 2628–2644. https://doi.org/10.1175/1520-0442(1998)011<2628:iobaaf>2.0.co;2;2

Zhang, S., Lü, S., Bao, Y., & Ma, D. (2015). Sensitivity of precipitation over China to different cumulus parameterization schemes in RegCM4. *Journal of Meteorological Research*, *29*(1), 119–131. https://doi.org/10.1007/s13351-014-4042-2

Zhang, X., Huang, A., Dai, Y., Li, W., Gu, C., Yuan, H., et al. (2022). Influences of 3D sub-grid terrain radiative effect on the performance of CoLM over Heihe River Basin, Tibetan Plateau. *Journal of Advances in Modeling Earth Systems*, *14*(1), e2021MS002654. https://doi.org/10.1029/2021MS002654

Zhang, Y., Huang, A., & Zhu, X. (2006). Parameterization of the thermal impacts of sub-grid orography on numerical modeling of the surface energy budget over East Asia. *Theoretical and Applied Climatology*, *86*(1–4), 201–214. https://doi.org/10.1007/s00704-005-0209-1

Zhao, P., Xu, X., Chen, F., Guo, X., Zheng, X., Liu, L., et al. (2018). The third atmospheric scientific experiment for understanding the Earth-atmosphere coupled system over the Tibetan Plateau and its effects. *Bulletin of the American Meteorological Society*, *99*(4), 757–776. https://doi.org/10.1175/bams-d-16-0050.1

Zhao, Y., Zhou, T., Li, P., Furtado, K., & Zou, L. (2021). Added value of a convection permitting model in simulating atmospheric water cycle over the Asian water tower. *Journal of Geophysical Research: Atmospheres*, *126*(13). https://doi.org/10.1029/2021JD034788

Zheng, J., Bian, J., Ge, Q., Hao, Z., Yin, Y., & Liao, Y. (2013). The climate regionalization in China for 1981–2010 (in Chinese with English abstract). *Chinese Science Bulletin (Chinese Version)*, *58*(30), 3088–3099. https://doi.org/10.1360/972012-1491

Zhong, R., Zhao, T., He, Y., & Chen, X. (2019). Hydropower change of the water tower of Asia in 21st century: A case of the Lancang River hydropower base, upper Mekong. *Energy*, *179*, 685–696. https://doi.org/10.1016/j.energy.2019.05.059

Zhou, X., Yang, K., Beljaars, A., Li, H., Lin, C., Huang, B., & Wang, Y. (2019). Dynamical impact of parameterized turbulent orographic form drag on the simulation of winter precipitation over the western Tibetan Plateau. *Climate Dynamics*, *53*(1–2), 707–720. https://doi.org/10.1007/s00382-019-04628-0

Zhou, X., Yang, K., Ouyang, L., Wang, Y., Jiang, Y., Li, X., et al. (2021). Added value of kilometer-scale modeling over the third pole region: A CORDEX-CPTP pilot study. *Climate Dynamics*, *57*(7), 1673–1687. https://doi.org/10.1007/s00382-021-05653-8

Zhou, X., Yang, K., & Wang, Y. (2017). Implementation of a turbulent orographic form drag scheme in WRF and its application to the Tibetan Plateau. *Climate Dynamics*, *50*(7–8), 2443–2455. https://doi.org/10.1007/s00382-017-3677-y

Zhu, Y.-Y., & Yang, S. (2020). Evaluation of CMIP6 for historical temperature and precipitation over the Tibetan Plateau and its comparison with CMIP5. *Advances in Climate Change Research*, *11*(3), 239–251. https://doi.org/10.1016/j.accre.2020.08.001

Zou, J., Xie, Z., Qin, P., Ma, Q., & Sun, Q. (2013). Changes of terrestrial water storage in river basins of China projected by RegCM4. *Atmospheric and Oceanic Science Letters*, *6*(3), 154–160. https://doi.org/10.3878/j.issn.1674-2834.13.0011